2005

Heavy Metal Complexes of Mixed S,N Donor Ligands: X-Ray Crystallography and Solution-State 1H NMR

Wei Lai
College of William & Mary - Arts & Sciences

HEAVY METAL COMPLEXES OF MIXED S,N DONOR LIGANDS

X-Ray Crystallography and Solution-State ^{1}H NMR

A Thesis

Presented to

The Faculty of the Department of Chemistry

The College of William and Mary in Virginia

In Partial Fulfillment

Of the Requirements for the Degree of

Master of Science

By

Wei Lai

2005

APPROVAL SHEET

This thesis is submitted in partial fulfillment of

the requirements for the degree of

Master of Science

Wei Lai

Approved by the Committee, July 2005

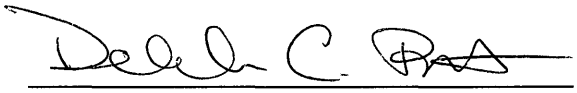

Deborah C. Bebout, Chair

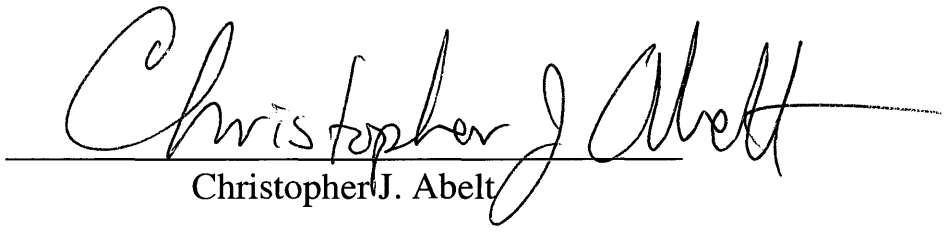

Christopher J. Abelt

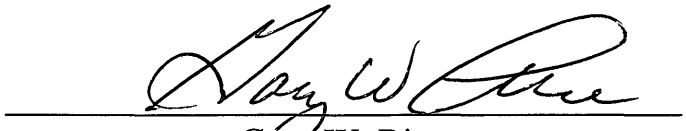

Gary W. Rice

TABLE OF CONTENTS

ACKNOWLEDGEMENTS

I would like to give my deep thanks to Dr. Bebout, my research advisor, for her teaching and guidance throughout this research work. It was a great experience to learn from her. I was deeply inspired by her scientific sense and hard work with boundless enthusiasm.

My thanks to Dr. Abelt and Dr. Rice for serving as my committee members, and for their contributions to this manuscript.

During my research work, I was very pleased to work with Dr. Berry. He spent much time teaching me the instrumental techniques and discussing the scientific problems with me. I appreciate his collaboration and enormous help.

I also would like to express my appreciation to the Department of Chemistry for financial support. My thanks to the entire Bebout group who have made contributions to my work through experimental assistance. My thanks also to Dr. Butcher for X-ray characterization.

Finally, a special thank you to my husband, Yonglai Yang for his love, support and encouragement.

This work was partially supported by the National Science Foundation and the American Chemical Society Petroleum Research Fund.

LIST OF TABLES

LIST OF FIGURES

ABSTRACT

The binding of heavy metals (Hg(II), Cd(II), Zn(II), and Pb(II)) to the mixed nitrogen and sulfur donor ligands 2,6-bis(methylthiomethyl)pyridine($\mathbf{L_1}^1$), N-(2-pyridylmethyl)-N-(2-(methylthio)ethyl)amine ($\mathbf{L_2}$) and N-(2-pyridylmethyl)-N-(2-(methylthio)ethyl)-N-(2-thioethyl)amine ($\mathbf{L_3}$) were investigated by X-ray crystallography and ^{1}H NMR spectroscopy. These ligands all contain pyridine and thioether donating groups to model protein environments containing histidine and methionine amino acid residues.

Thirteen heavy metal complexes with $\mathbf{L_1}^1$, $\mathbf{L_2}$ or $\mathbf{L_3}$ were synthesized and characterized by X-ray crystallography and solution-state ^{1}H NMR spectroscopy. The distorted meridional octahedral $M(\mathbf{L_1}^1)_2(ClO_4)_2$ series includes the first structurally characterized Zn(II) and Cd(II) complexes with $N_2(SR_2)_4$ coordination spheres. Coordination of $HgCl_2$ and $ZnCl_2$ with one molar equivalent of ligand afforded mononuclear, five coordinate species $Hg(\mathbf{L_1}^1)Cl_2$ and $Zn(\mathbf{L_1}^1)Cl_2$, with distorted square pyramidal and trigonal bipyramidal geometries, respectively. The 1:1 chloride Cd(II):$\mathbf{L_1}^1$ complex exists at the solid-state as the dimer $[Cd_2(\mathbf{L}^1)_2Cl_4]$ with a distorted octahedral geometry. The trans facial octahedral $M(\mathbf{L_2})_2(ClO_4)_2$ series was prepared by slow diffusion. Complex $Zn(\mathbf{L_2})Cl_2$ was also synthesized for comparison with the known complexes $Hg(\mathbf{L_2})Cl_2$ and $Cd(\mathbf{L_2})Cl_2$. Multinuclear complexes $Hg_4(\mathbf{L_3})_4(ClO_4)_4\cdot$6acetone and $Cd_3(\mathbf{L_3})_3(CO_3)(ClO_4)\cdot 0.5H_2O$ were also characterized crystallographically.

^{1}H NMR spectral trends indicated that the ligand exchange rate of $[M(\mathbf{L_1}^1)_2]^{2+}$ increased in the order Hg(II) < Zn(II) < Cd(II)<Pb(II). Slow exchange conditions on the chemical shift time scale were found for 1:2 metal-to-ligand complexes of $\mathbf{L_1}^1$ with Hg(II) and Zn(II) but not Cd(II) and Pb(II). Slow exchange conditions in acetonitrile-d_3 solutions permitting detection of $^{3\text{-}5}J(^{199}Hg^1H)$ were found for 1:1 and 1:2 $Hg(ClO_4)_2$:$\mathbf{L_1}^1$ complexes, but not for the related $Cd(ClO_4)_2$ and $Pb(ClO_4)_2$ complexes. Slow exchange conditions on the chemical shift time scale were also found for the 1:1 and 1:2 $M(ClO_4)_2$:$\mathbf{L_2}$ complexes. Slow exchange conditions on the coupling constant time scale allowed the detection of $J(^{199}Hg^1H)$ and $J(^{113}Cd^1H)$ for 1:1 and 1:2 Hg(II) and Cd(II) complexes with $\mathbf{L_2}$. The relative stability of the zinc triad complexes of $\mathbf{L_1}^1$ suggests that the toxicity of Hg(II) is accentuated by the relative difficulty of displacing it from the coordination sites encountered. Due to the tendency of ^{199}Hg to exhibit larger and longer range heteronuclear coupling constants, ^{199}Hg NMR methods appear to have some significant advantages as metallobioprobes over ^{113}Cd NMR methods.

HEAVY METAL COMPLEXES OF MIXED S,N DONOR LIGANDS

INTRODUCTION

Investigations of the molecular mechanisms of toxicity for heavy metals such as Hg, Cd and Pb are active areas of research due to the detrimental effects of these metals on human beings and higher organisms. Not only are compounds of these metals typically highly toxic, but also they tend to accumulate in higher organisms.[1] It is believed that these metal ions impact protein structures either by substitution of the native metal of metalloproteins or by thermodynamically trapping proteins in misfolded states. Protein metal-binding sites containing certain structural motifs are believed to be the potential targets for perturbation by these heavy metals.[2] Protein metal binding sites typically contain three to six oxygen, nitrogen, and/or sulfur donors depending on the identity of the native metal ion and its function. The tertiary structure of the protein imposes a specific orientation on the donor atoms, which serves to both enhance selectivity for the correct metal ion and provide the appropriate electronic environment to facilitate the desired chemistry. As a result, protein metal binding sites are highly selective for a single physiologically essential metal ion in normal circumstances. For instance, in physiological systems, Zn(II) serves important catalytic and structural roles by selectively binding to sites of specific metalloproteins. Although the molecular mechanisms for the toxicities of heavy metal ions are incompletely understood, the low coordination geometry and number preferences of Cd(II), Hg(II) and Pb(II) undoubtedly contribute to their ease of substitution for a variety of native metal ions. Lead has been proved to interfere with the metabolism and action of essential metals such as Ca, Fe and Zn.[3] Recently cadmium was identified as an essential element for the marine diatom *Thalassiosira weissflogii* which synthesizes a novel Cd(II)-specific carbonic anhydrase

under conditions where zinc is scarce.[4] Other than Hg(II) binding to a protein responsible for transcriptional regulation of mercury detoxification proteins, no physiologically beneficial roles have been discovered for Hg(II). However, the other group 12 metal, zinc, acts an essential trace element specifically utilized by many enzymes in biological system. The considerable differences between the bioactivities of group 12 metal ions motivate their parallel investigations.

Since the behavior of these toxic metal ions in proteins cannot be separated from the fundamental chemistry of the particular metal, studies of synthetic complexes with small biologically relevant ligands have been useful. These complexes can be used to investigate the effects of systematic variations in coordination geometry, ligation, local environment, and other factors, often providing insights that cannot be easily attained from protein studies. In addition, globular protein molecules are large, spherical, or ellipsoidal objects with irregular surfaces, so well-ordered crystals of proteins are difficult to grow. Multidentate biologically relevant small ligands have been applied extensively to the synthesis of metal complexes because of their ease of preparation, wealth of spectroscopic and X-ray crystallographic data available for their metal complexes, and the predictable changes in the physical properties of the metal complex with variation in the ligand.

Table 1. Properties of NMR-active nuclei of Cd, Hg and Pb

Parameter	^{111}Cd	^{113}Cd	^{199}Hg	^{201}Hg	^{207}Pb
Spin	1/2	1/2	1/2	3/2	1/2
Natural abundance	12.75	12.26	16.84	13.22	22.6
Relative receptivity	6.97	7.59	5.42	1.08	11.8
Chemical shift range (ppm)		900	5000		16000

However, investigating the coordination chemistry of these metal ions poses some unique challenges. The divalent forms of these metals are d^{10} and therefore their coordination number and geometry preferences are considerably less strong than most other metal ions. As a result, their coordination chemistry with simple ligands is plagued by complex speciation and rapid exchange. Clarification of the range of slow exchange binding environments for the divalent heavy metal ions is required to fully appreciate the intricate coordination of specific metal binding events in biochemistry and the potentially most detrimental physiological effects of heavy metal ions. Also, these divalent metal ions are diamagnetic and there are few spectroscopies available for studying their coordination. Perhaps the most versatile spectroscopic method for characterizing organic complexes of these metals is Nuclear Magnetic Resonance (NMR), which can detect slow ligand exchange on both the chemical shift and on the $J(^{111/113}Cd^{1}H)$, $J(^{199}Hg^{1}H)$ and $J(^{207}Pb^{1}H)$ time scales for Cd(II), Hg(II) and Pb(II) complexes, respectively. Table 1 lists the natural abundance, relative receptivity (compared to ^{13}C) of the NMR-active nuclei of these three metals. ^{201}Hg is quadrupolar, leading to excessive line broadening that precludes routine observation. ^{113}Cd is typically used in direct observation experiments due to its higher receptivity compared to ^{111}Cd. In addition, the large range chemical shift of ^{113}Cd, ^{199}Hg and ^{207}Pb NMR can provide information regarding the number and type of ligand atoms, as well as coordination geometry.[5,6] Furthermore, the heteronuclear couplings between the ligand protons and ^{119}Hg and $^{111/113}Cd$ observed by ^{1}H NMR have provided valuable information regarding ligand coordination to these metal ions in solution state.[7-13] In previous studies, the solid- and solution-state coordination chemistry of divalent mercury and cadmium ions with a variety of bidentate

and tridentate ligands have been investigated by X-ray crystallography and ^{1}H NMR. Slow exchange on the coupling constant time scale has permitted detection of heteronuclear couplings between ^{199}Hg and ^{1}H over as many as five-bonds.[9,14]

On the other hand, because of their favorable NMR properties and low coordination geometry preference, ^{199}Hg, ^{113}Cd and ^{207}Pb occupy a position of preeminence in probing metal-binding sites where the native physiological metal ions can be substituted with these spin I = ½ metal isotopes. Approximately one third of all proteins require metal interactions for complete physiological activity and they constitute about 3% of human body weight. These metal ions may facilitate protein folding or be directly involved with the chemistry at the active site of a protein. NMR is one of the most powerful spectroscopic techniques because it can provide specific bonding information, but none of the physiologically essential metal ions has an isotope with favorable NMR properties. Identification of the specific amino acids involved in a protein metal binding site is greatly facilitated by detection of $J(M^{1}H)$. Therefore, detailed NMR information about protein metal binding sites requires metal substitution. The ideal metallobioprobe would have similar coordination properties to the native metal ion yet offer a sensitive alternative means of protein characterization. The conformational flexibility of d^{10} metal ions makes them ideal candidates for certain protein metal substitution studies. Extensive studies have shown ^{113}Cd NMR is a powerful structural probe of zinc, calcium and copper proteins metal binding sites.[6] Although NMR studies of ^{199}Hg- and ^{207}Pb-substituted proteins are currently limited,[5,15-18] the different donor atom preferences of Cd(II), Hg(II) and Pb(II) suggest that ^{199}Hg and ^{207}Pb NMR methods would complement ^{113}Cd NMR methods. In addition, ^{199}Hg has shorter relaxation times,

larger and longer range heteronuclear coupling constants and greater chemical shift dispersion in comparison with ^{113}Cd NMR. ^{207}Pb exhibits a moderate resonance frequency, a vast chemical shift range and potentially even larger heteronuclear couplings. Hg(II) and Pb(II) are slightly larger than Cd(II) and significantly larger than the physiological essential metal ions. However, Hg(II) has been substituted for native Fe(II),[19] Cu(II),[5,15,16] and Zn(II)[20,21] ions without significant changes in overall protein structure or identity of the metal ligands. To our knowledge, no structurally characterized Pb(II) substituted metalloproteins have been reported. The dependence of the ^{207}Pb NMR parameters upon the Pb(II) coordination environment needs to be systematically investigated.

Sulfur/nitrogen mixed donor ligands, such as macrocyclic thioethers and thiolates, have been widely used to investigate d^{10} metal binding properties in part due to the affinity of the amino acid cysteine and histidine for heavy metals,[22-26] however their complexes of acyclic thiother ligands have been less studied. So, in this work, X-ray crystallographic and solution-state ^1H NMR characterization of the coordination chemistry of divalent d^{10} metal ions with tridentate or tetradentate mixed sulfur and nitrogen donor ligands 2,6-bis(methythiomethyl)pyridine ($\mathbf{L_1^1}$), N-(2-pyridylmethyl)-N-(2-(methylthio)ethyl)amine ($\mathbf{L_2}$) and N-(2-pyridylmethyl)-N-(2-(methylthio)ethyl)-N-(2-thioethyl)amine ($\mathbf{L_3}$) are reported.

2,6-Bis(methythiomethyl)pyridine($\mathbf{L_1^1}$) has an SNS-donor set. As summarized in Figure 1, several other dithioether derivatized lutidyl ligands have been previously reported.[27-35] In crystallographically characterized metal complexes, these ligands generally behave as tridentate chelating ligands, giving two five-membered rings.[27,29,34,35]

Bidentate binding modes have been observed in $[Pd(Me)(\mathbf{L_1}^1)]$[31] and $[Cu(\mathbf{L_1}^3)Br(\mu\text{-}Br)]_2$[27] where only the pyridine nitrogen and one thioether moiety bind the metal ions. The only group 12 metal ion complexes previously reported with this family of ligands are $[Zn(\mathbf{L_1}^2)Br_2]$[35] and $[Cd(\mathbf{L_1}^2)Cl(\mu\text{-}Cl)]_2$.[33] In this work, seven crystal structures of $\mathbf{L_1}^1$ complexes with Hg(II), Cd(II), Zn(II) and Pb(II) are presented. X-ray crystallographic structures are presented for nonhomologous chloride complexes with 1:1 metal-to-ligand stoichiometry and for a homologous $[M(\mathbf{L_1}^1)_2](ClO_4)_2$ series for Hg(II), Cd(II) and Zn(II). Due to higher affinity for oxygen, Pb(II) coordinates to two perchlorate oxygen atoms in the complex $[Pb(\mathbf{L_1}^1)_2(ClO_4)_2]$, leading to a different coordinate environment for Pb(II) in comparison with the group 12 metals. These are the first complexes with stoichiometry $M(\mathbf{L_1})_2$ with this class of ligands, and the first complexes of Zn(II) and Cd(II) with $N_2(SR_2)_4$ coordination spheres, to be crystallographically characterized. Conditions for slow ligand exchange on the chemical shift time scale in acetonitrile-d_3 solution were found for $[Zn(\mathbf{L_1}^1)_2]^{2+}$ and $[Hg(\mathbf{L_1}^1)_2]^{2+}$, but not $[Cd(\mathbf{L_1}^1)_2]^{2+}$ and $[Pb(\mathbf{L_1}^1)_2](ClO_4)_2$. In addition, slow exchange conditions on the $J(M^1H)$ time scale were found for $[Hg(\mathbf{L_1}^1)_2]^{2+}$ and $[Hg(\mathbf{L_1}^1)(CH_3CN)_x]^{2+}$ but neither of the comparable Cd(II) and Pb(II) complexes. The slowest exchange rates were observed for this SNS ligand with Hg(II), followed by Zn(II) and finally Cd(II) and Pb(II). This observation suggests that the relative difficulty of displacing Hg(II) from mixed nitrogen, sulfur coordination environments contributes to the broad toxicological effects of Hg(II).

As shown in Figure 2, N-(2-pyridylmethyl)-N-(2-(methylthio)ethyl)amine ($\mathbf{L_2}$) and N-(2-pyridylmethyl)-N-(2-(methylthio)ethyl)-N-(2-thioethyl)amine ($\mathbf{L_3}$) are structurally related. As the precursor of $\mathbf{L_3}$, $\mathbf{L_2}$ is a secondary amine containing NNS

donor atoms. $\mathbf{L_3}$ is a tertiary amine containing a NNSS donor atom set that includes a thiol group in addition to those present in $\mathbf{L_2}$. Significantly, $\mathbf{L_2}$ and $\mathbf{L_3}$ have low symmetry and each donor group is unique.

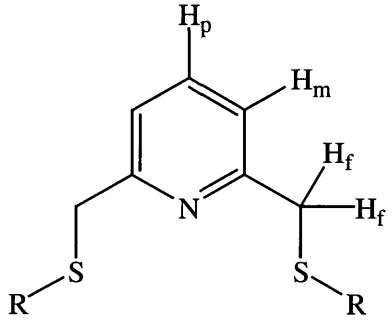

L_1^1: R = CH_{3g}
L_1^2: R = Ethyl
L_1^3: R = Benzyl
L_1^4: R = CH_2Ph
L_1^5: R = CH_2CH_2Ph
L_1^6: R = t-Butyl
L_1^7:R = PhCOOMe
L_1^8: R = PhCOOEt
L_1^9: R = PhCl

Figure 1. Structure of dithioether derivatized lutidyl ligands

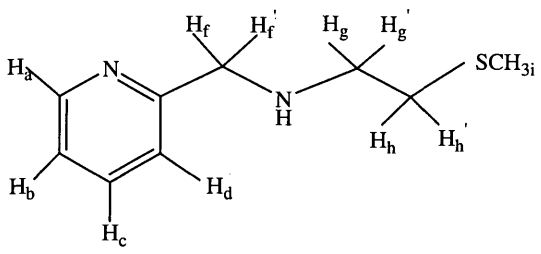

L_2

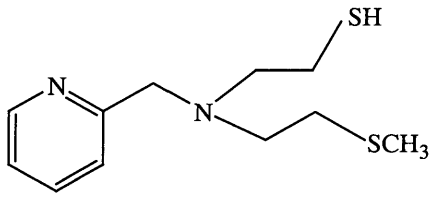

L_3

Figure 2. Structures of N-(2-pyridylmethyl)-N-(2-(methylthio)ethyl)amine ($\mathbf{L_2}$) and N-(2-pyridylmethyl)-N-(2-(methylthio)ethyl)-N-(2-thioethyl)amine ($\mathbf{L_3}$)

Four crystal structures of $\mathbf{L_2}$ complexes with group 12 metal ions are presented in this work. $Hg(\mathbf{L_2})Cl_2$ and $Cd(\mathbf{L_2})Cl_2$ have previously been synthesized in our group.[36] Previous attempts to crystallize complexes with stoichiometry $[M(\mathbf{L_2})_2]^{2+}$ by slow evaporation yielded only oils. However, using slow diffusion, a series of homologous

$[M(\mathbf{L_2})_2](ClO_4)_2$ complexes (M = Hg, Cd, Zn) have been successfully crystallized. Complex $Zn(\mathbf{L_2})Cl_2$ has also been synthesized for comparison. Similar to $M(\mathbf{L_1}^1)Cl_2$, the three chloride complexes $M(\mathbf{L_2})Cl_2$ (M = Hg, Cd, Zn) are nonhomologous with $Cd(\mathbf{L_2})Cl_2$ existing at the solid-state as a polymer. Similar to $\mathbf{L_1}^1$, tridentate coordination of $\mathbf{L_2}$ produces a complex with two five-membered rings. The solution state coordination chemistry of $\mathbf{L_2}$ was similar with the divalent zinc triad metal ions. Slow exchange on the chemical shift time scale was observed for the 1:1 and 1:2 metal-to-ligand complexes of $\mathbf{L_2}$ with Hg(II), Cd(II) and Zn(II). Slow exchange on the $J(M^1H)$ time scale were observed for 1:1 and 1:2 metal-to-ligand complexes of $\mathbf{L_2}$ with Hg(II) and Cd(II). The similarity in the solid- and solution-state coordination chemistry of the divalent group 12 metal ions revealed that Hg(II) and Cd(II) may serve as appropriate metallobioprobes of biological Zn(II) coordination environments and further substantiates the toxicological potential of their substitution of Zn(II) proteins.

Nonhomologous polymeric Hg(II) and Cd(II) complexes with $\mathbf{L_3}$ were prepared and characterized crystallographically. A tridentate bonding mode with pendant thioether was observed in $[Cd_3(\mathbf{L_3})_3(CO_3)](ClO_4)\cdot 0.5H_2O$. In contrast, a tetradentate bonding mode involving all the donor groups was observed in $[Hg_4(\mathbf{L_3})_4](ClO_4)_4\cdot$6acetone. Solution-state NMR studies with $\mathbf{L_3}$ were not successful due to facile ligand dimerization to form a disulfide.

EXPERIMENTAL

Methods and Materials. Solvents and reagents were of commercial grade and used as received unless otherwise stated. Elemental analyses were carried out by Atlantic Microlab, Inc., Norcross, Georgia. Reported coupling constants are interproton unless otherwise noted. *Caution!* All of the perchlorate salts of metal complexes included in this work were stable for routine synthesis and purification procedures. However, organic perchlorates are potentially explosive and should be handled with care.[37]

Solution-state NMR Spectroscopy. NMR spectra were collected in 5 mm o.d. NMR tubes on a Varian Mercury 400VX NMR spectrometer operating in the pulse Fourier transform mode. All solutions for low temperature NMR measurements were prepared in 650 μL CD_3CN by adding stock solutions of 10 mM metal salt to a solution of 20 mM ligand. The metal ion concentration in the solution used in the NMR analysis was nominally 2 mM, and the ratio of metal ion to the ligand varied between 0.125 and 1.75. The sample temperature was maintained by blowing chilled nitrogen over the NMR tube in the probe. Proton chemical shifts were measured relative to internal solvent but are reported relative to tetramethylsilane (TMS).

X-ray Crystallography. Selected crystallographic data are given in Tables 2-8. Data were collected on a Siemens P4 four-circle diffractometer using a graphite-monochromated Mo Kα X-radiation (λ = 0.710 73 Å). During data collection three standard reflections were measured after every 97 reflections. The structures were solved by direct methods and refined on F^2 by full-matrix least squares using the SHELXTL97 program package.[38] All non-hydrogen atoms were fixed as anisotropic, the hydrogen

atomic positions were fixed relative to the bonded carbons, and the isotropic thermal parameters were fixed.

Table 2. Crystallographic data for complexes **1** and **2**

complex	$Hg(\mathbf{L_1}^1)_2(ClO_4)_2$ **(1)**	$Cd(\mathbf{L_1}^1)_2(ClO_4)_2$ **(2)**
empirical formula	$C_{18}H_{26}Cl_2HgN_2O_8S_4$	$C_{18}H_{26}CdCl_2N_2O_8S_4$
fw	798.14	709.95
crystal system	orthorhombic	orthorhombic
space group	Ibca	Pcca
a, Å	13.5814(17)	14.2898(19)
b, Å	14.184(3)	13.5492(17)
c, Å	27.412(3)	27.536(4)
α, deg	90	90
β, deg	90	90
γ, deg	90	90
V, Å^3	5280.5(14)	5331.4(12)
Z	8	8
d_{calc}, g cm^{-3}	2.008	1.769
μ, mm^{-1}	6.394	1.378
T, K	148(2)	103(2)
R1,[a] wR2[b] [$I > 2\sigma(I)$]	0.0452, 0.1026	0.0234, 0.0582
R1,[a] wR2[b] (all data)	0.0597, 0.1115	0.0377, 0.0613

[a] $R1 = \Sigma||F_o| - |F_c||/\Sigma|F_o|$. [b] $wR2 = [\Sigma[w(F_o^2 - F_c^2)^2]/\Sigma[w(F_o^2)^2]]^{1/2}$

Table 3. Crystallographic data for complexes **3** and **4**

complex	$Zn(\mathbf{L_1}^1)_2(ClO_4)_2$ (**3**)	$Hg(\mathbf{L_1}^1)Cl_2$ (**4**)
empirical formula	$C_{18}H_{26}Cl_2N_2O_8S_4Zn$	$C_9H_{13}Cl_2\,HgNS_2$
fw	662.92	470.81
crystal system	monoclinic	triclinic
space group	$P2_1/n$	P-1
a, Å	11.982(6)	7.57(2)
b, Å	11.667(6)	7.84(2)
c, Å	19.559(11)	11.67(3)
α, deg	90	87.92(2)
β, deg	103.672(9)	83.39(5)
γ, deg	90	81.87(5)
V, Å^3	2657(2)	681(3)
Z	4	2
d_{calc}, g cm^{-3}	1.657	2.297
μ, mm^{-1}	1.485	11.975
T, K	103(2)	148(2)
R1,[a] wR2[b] [$I > 2\sigma(I)$]	0.0396, 0.0974	0.0820, 0.2255
R1,[a] wR2[b] (all data)	0.0605, 0.1080	0.0877, 0.2320

[a] $R1 = \Sigma||F_o| - |F_c||/\Sigma|F_o|$. [b] $wR2 = [\Sigma[w(F_o^2 - F_c^2)^2]/\Sigma[w(F_o^2)^2]]^{1/2}$

Table 4. Crystallographic data for complexes **5** and **6**

complex	$[Cd_2(\mathbf{L_1}^1)_2Cl_4]$ (**5**)	$Zn(\mathbf{L_1}^1)Cl_2$ (**6**)
empirical formula	$C_{18}H_{26}Cd_2Cl_4N_2S_4$	$C_9H_{13}Cl_2NS_2Zn$
fw	765.25	335.59
crystal system	monoclinic	orthorhombic
space group	$P2_1$	$P2_12_12_1$
a, Å	7.8108(13)	15.090(6)
b, Å	14.487(3)	15.121(6)
c, Å	11.835(2)	11.663(5)
α, deg	90	90
β, deg	103.095(3)	90
γ, deg	90	90
V, Å^3	1304.3(4)	2661.2(19)
Z	2	8
d_{calc}, g cm^{-3}	1.948	1.675
μ, mm^{-1}	2.371	2.529
T, K	148(2)	103(2)
R1,[a] wR2[b] [$I > 2\sigma(I)$]	0.0332, 0.0862	0.0172, 0.0405
R1,[a] wR2[b] (all data)	0.0340, 0.0869	0.0187, 0.0410

[a] $R1 = \Sigma||F_o| - |F_c||/\Sigma|F_o|$. [b] $wR2 = [\Sigma[w(F_o^2 - F_c^2)^2]/\Sigma[w(F_o^2)^2]]^{1/2}$

Table 5. Crystallographic data for complexes **7** and **8**

complex	$Pb(\mathbf{L_1}^1)_2(ClO_4)_2$ (**7**)	$Hg(\mathbf{L_2})_2(ClO_4)_2$ (**8**)
empirical formula	$C_{18}H_{26}Cl_2N_2O_8PbS_4$	$C_{18}H_{28}Cl_2HgN_4O_8S_2$
fw	804.74	764.05
crystal system	Triclinic	Monoclinic
space group	P-1	P2(1)/c
a, Å	9.2080(7)	8.116(5)
b, Å	9.0098(7)	13.048(8
c, Å	17.7418(15)	12.213(7)
α, deg	86.9690(10)	90
β, deg	78.2040(10)	107.596(10)
γ, deg	65.1060(10)	90
V, Å^3	1306.03(18)	1232.7(12)
Z	2	2
d_{calc}, g cm^{-3}	2.046	2.058
μ, mm^{-1}	7.030	6.682
T, K	93(2)	93(2)
R1,[a] wR2[b] [$I > 2\sigma(I)$]	0.0344, 0.0878	0.0224, 0.0571
R1,[a] wR2[b] (all data)	0.0359, 0.0890	0.0251, 0.0587

[a] $R1 = \Sigma||F_o| - |F_c||/\Sigma|F_o|$. [b] $wR2 = [\Sigma[w(F_o^2 - F_c^2)^2]/\Sigma[w(F_o^2)^2]^{1/2}$

Table 6. Crystallographic data for complexes **9** and **10**

complex	$Cd(\mathbf{L_2})_2(ClO_4)_2 \cdot H_2O$ (**9**)	$Zn(\mathbf{L_2})_2(ClO_4)_2 \cdot H_2O$ (**10**)
empirical formula	$C_{18}H_{30}CdCl_2N_4O_9S_2$	$C_{18}H_{30}Cl_2N_4O_9S_2Zn$
fw	693.88	646.85
crystal system	Monoclinic	Monoclinic
space group	C2/c	C2/c
a, Å	20.807(8)	21.472(16)
b, Å	10.357(4)	10.014(6)
c, Å	13.487(5)	13.625(12)
α, deg	90	90
β, deg	115.659(6)	119.36(2)
γ, deg	90	90
V, Å^3	2619.8(17)	2553(3)
Z	4	4
d_{calc}, g cm^{-3}	1.759	1.683
μ, mm^{-1}	1.251	1.391
T, K	93(2)	93(2)
R1,[a] wR2[b] [$I > 2\sigma(I)$]	0.0257, 0.0633	0.0267, .0669
R1,[a] wR2[b] (all data)	0.0278, 0.0647	0.0304, .0690

[a] $R1 = \Sigma||F_o| - |F_c||/\Sigma|F_o|$. [b] $wR2 = [\Sigma[w(F_o^2 - F_c^2)^2]/\Sigma[w(F_o^2)^2]]^{1/2}$

Table 7. Crystallographic data for complexes **11**and **12**

complex	$Zn(\mathbf{L_2})Cl_2$ (**11**)	$Hg_4(\mathbf{L_3})_4(ClO_4)_4 \cdot 6$acetone (**12**)
empirical formula	$C_9H_{14}Cl_2N_2SZn$	$C_{62}H_{104}Cl_4Hg_4N_8O_{22}S_8$
fw	318.55	2514.17
crystal system	Triclinic	Monoclinic
space group	P-1	C2/c
a, Å	8.2003(13)	20.275(3)
b, Å	8.2331(14)	14.2040(19)
c, Å	10.5696(17)	30.686(4)
α, deg	109.505(3)	90
β, deg	102.713(3)	101.084(2)
γ, deg	101.841(3)	90
V, Å^3	625.29(18)	8672(2)
Z	2	4
d_{calc}, g cm^{-3}	1.692	1.926
μ, mm^{-1}	2.527	7.445
T, K	93(2)	93(2) K
R1,[a] wR2[b] [$I > 2\sigma(I)$]	0.0253, 0.0643	0.0276, 0.0588
R1,[a] wR2[b] (all data)	0.0281, 0.0657	0.0358, 0.0619

[a] $R1 = \Sigma||F_o| - |F_c||/\Sigma|F_o|$. [b] $wR2 = [\Sigma[w(F_o^2 - F_c^2)^2]/\Sigma[w(F_o^2)^2]^{1/2}$

Table 8. Crystallographic data for complex **13**

complex	$Cd_3(\mathbf{L_3})_3(CO_3)(ClO_4)\cdot 0.5H_2O$ (**13**)
empirical formula	$C_{34}H_{52}Cd_3ClN_6O_7S_6$
fw	1229.83
crystal system	Rhombohedral
space group	R-3
a, Å	13.181(10)
b, Å	13.181(10)
c, Å	43.83(6)
α, deg	90
β, deg	90
γ, deg	120
V, Å^3	6594(11)
Z	6
d_{calc}, g cm^{-3}	1.858
μ, mm^{-1}	*1.838*
T, K	103(2) K
R1,[a] wR2[b] [$I > 2\sigma(I)$]	0.0288, 0.0674
R1,[a] wR2[b] (all data)	0.0406, 0.0713

[a] $R1 = \Sigma||F_o|\text{-}\ |F_c||/\Sigma|F_o|$. [b] $wR2 = [\Sigma[w(F_o^2 - F_c^2)^2]/\Sigma[w(F_o^2)^2]]^{1/2}$

Synthesis of 2,6-bis(methythiomethyl)pyridine (L_1^1). The ligand was prepared by variation of the procedure described by Canovese and coworkers.[39] Sodium methanethiolate (3.1 g, 44 mmol) was added to an ice-cooled solution of 2,6-bis(bromomethyl)pyridine[40] (5.28 g, 20 mmol) in DMF (50 ml). The mixture was brought to room temperature and stirred for 24 h. The solvent was removed by Kugelrohr distillation (50 °C, 0.5 mmHg). Continued Kugelrohr distillation (150 °C, 0.01 mmHg) of the yellow oily residue yielded $\mathbf{L_1^1}$ as a colorless oil (3.30 g, 83%). ^{1}H NMR (CD_3CN, 20 °C): δ 2.07(s, 6H, H_g), 3.75 (s, 4H, H_f), 7.26 (d, 2H, J = 8 Hz, H_m), 7.70 (t, 1H, J = 8 Hz, H_p). Anal. Calcd for $C_9H_{13}NS_2$: C, 27.09; H, 3.28; N, 3.51. Found: C, 27.09; H, 3.27; N, 3.53.

Synthesis of N-(2-pyridylmethyl)-N-(2-(methylthio)ethyl)amine (L_2). This ligand was prepared according to an adaption of the procedure published by Tyeklar et al.[41] A solution of 2-chloroethyl methyl sulfide (2.4 ml, 24 mmol) in 20 mL deionized water was cooled to 0 °C in an acid bath. To this solution was added slowly with stirring a solution of 2-(aminomethyl)pyridine (2.10 mL, 20 mmol) in 35 mL methylene chloride. The mixture was then allowed to warm to room temperature. Over a 48-hour period, 12 mL of 2 M NaOH was added by syringe pump. According to the literature, the reaction should remain basic, but not exceed a pH of 9.5. The crude mixture was washed with 40 mL of 4M NaOH, and the organic phase was dried with sodium sulfate and filtered. Removal of methylene chloride yielded a brown liquid. Fractional vacuum distillation yielded $\mathbf{L_2}$ as a colorless oil (1.802 g, 49%). ^{1}H NMR (CD_3CN, –40 °C): δ 2.02 (s, 3H, H_i), 2.62 (t, 2H, J = 7 Hz, H_h), 2.73 (t, 2H, J = 7 Hz, H_g), 3.83 (s, 2H, H_f), 7.23 (dd, 1H, J = 7, 5 Hz, H_b), 7.37 (d, 1H, J = 8, H_d), 7.72 (td, 1H, J = 8, 2 Hz, H_c), 8.51 (d, 1H, J = 5

Hz, H_a). Anal. Calcd for $C_9H_{14}N_2S$: C, 59.30; H, 7.74; N, 15.37. Found: C, 57.97; H, 7.80; N, 15.00.

Synthesis of N-(2-pyridylmethyl)-N-(2-(methylthio)ethyl)-N-(2-thioethyl)-amine (L_3). This procedure was adapted from that reported to synthesize the related ligand MEPAH (N-(2-Mercaptoethyl)picolylamine).[26] A 16 mL solution of freshly made N-(2-pyridylmethyl)-N-(2-(methylthio)ethyl)amine (8.5mmol, 1.56g) in toluene was brought to reflux. A solution of ethylene sulfide (9.35mmol, 0.56 g) in toluene was slowly added dropwise. The mixture was refluxed with stirring under argon for 24 h. The resulting orange solution was washed by water, dried with sodium sulfate and evaporated to dryness to give an oily product. Chromatography of this residue over alumina eluted with 3:1 ethyl acetate and hexanes yielded 1.22g of $\mathbf{L_3}$ (59%), as an yellow oil. ^{1}H NMR (CD_3CN, 20 °C): 2.05 (s, 3H), 2.62 (m, 4H), 2.74 (m, 4H), 3.78 (s, 2H), 7.22 (dd, 1H, J = 8, 5 Hz), 7.55 (d, 1H, J = 8 Hz), 7.73 (td, 1H, J = 8, 2 Hz), 8.49 (dm, 1H, J = 5 Hz). Anal. Calcd for $C_{11}H_{18}N_2S_2$: C, 54.50; H, 7.49; N, 11.56. Found: C, 55.04; H, 7.12; N, 11.42.

Preparation of $Hg(L_1^1)_2(ClO_4)_2$ (1). A solution of $Hg(ClO_4)_2{\cdot}3H_2O$ (227 mg, 0.5 mmol) in 5 mL methanol was added dropwise to a solution of $\mathbf{L_1^1}$ (100 mg, 0.5 mmol) in 5 mL methanol with stirring. A white precipitate formed. The solution was filtered and the filtrate was diluted slowly with 10 mL acetonitrile and set aside for slow evaporation. Colorless X-ray quality crystals of **1** (91.1 mg, 46%) formed upon standing for 4 days. Mp: 170–171 °C (dec). Anal. Calcd for $C_{18}H_{26}Cl_2HgN_2O_8S_4$: C, 54.26; H, 6.53; N, 7.03. Found: C, 54.43; H, 6.64; N, 7.01. ^{1}H NMR (2 mM, CD_3CN, 20 °C): δ 2.18 (s, 6H, $J(^{199}Hg^1H)$ = 49Hz, H_g), 4.15 (s, 4H, $J(^{199}Hg^1H)$ = 39 Hz, H_f), 7.54 (d, 2H, J = 8 Hz, $J(^{199}Hg^1H)$ = 13 Hz, H_m), 8.15 (t, 1H, J = 8 Hz, $J(^{199}Hg^1H)$ = 13 Hz, H_p).

Preparation of $Cd(L_1^1)_2(ClO_4)_2$ (2). A solution of $Cd(ClO_4)_2 \cdot 6H_2O$ (210 mg, 0.5 mmol) in 5 mL acetonitrile was added dropwise to a solution of L_1^1 (100 mg, 0.5 mmol) in 5 mL methanol with stirring. A white precipitate formed. The solution was clarified by the addition of 5 mL acetonitrile. The mixture was slowly diluted with 6 mL toluene and set aside for slow evaporation. Colorless X-ray quality crystals of **2** (102.0 mg, 57%) formed upon standing for 4 days. Mp: 248–250 °C (dec). Anal. Calcd for $C_{18}H_{26}CdCl_2N_2O_8S_4$: C, 30.46; H, 3.66; N, 3.95. Found: C, 30.41; H, 3.63; N, 3.88. ^{1}H NMR (2 mM, CD_3CN, 20 °C): δ 2.13 (s, 6H, H_g), 4.15 (s, 4H, H_f), 7.54 (d, 2H, J = 8 Hz, H_m), 8.01 (t, 1H, J = 8 Hz, H_p).

Preparation of $Zn(L_1^1)_2(ClO_4)_2$ (3). A solution of $Zn(ClO_4)_2 \cdot 6H_2O$ (186 mg, 0.5 mmol) in 3 mL acetone was added dropwise to a solution of L_1^1 (100 mg, 0.5 mmol) in 2 mL acetone with stirring. Colorless crystals of **3** (25.5 mg, 15%) suitable for X-ray crystallography were obtained in 5 mm glass tubes after 5 days by slow diffusion of the mixture into toluene. Mp: 229–231 °C. Anal. Calcd for $C_{18}H_{26}Cl_2N_2O_8S_4Zn$: C, 32.61; H, 3.95; N, 4.23. Found: C, 31.68; H, 3.94; N, 4.11. ^{1}H NMR (2 mM, CD_3CN, 20 °C): δ 2.10 (s, 6H, H_g), 4.07 (s, 4H, H_f), 7.51 (d, 2H, J = 7 Hz, H_m), 7.99 (t, 1H, J = 8 Hz, H_p).

Preparation of $Hg(L_1^1)Cl_2$ (4). A solution of $HgCl_2$ (136 mg, 0.5 mmol) in 5 mL methanol was added dropwise to a solution of L_1^1 (100 mg, 0.5 mmol) in 5mL acetonitrile with stirring. Slow evaporation of the solution resulted in formation of colorless X-ray quality crystals of **4** (90.0 mg, 38%) in 10 days. Mp: 132–133 °C. Anal. Calcd for $C_9H_{13}Cl_2HgNS_2$: C, 22.96; H, 2.78; N, 2.98. Found: C, 23.05; H, 2.75; N, 2.91. ^{1}H NMR (2 mM, CD_3CN, 20 °C): δ 2.05 (s, 6H, H_g), 4.14 (s, 4H, $4H_f$), 7.46 (d, 2H, J = 8 Hz, H_m), 7.93 (t, 1H, J = 8 Hz, H_p).

Preparation of $Cd_2(L_1^1)_2Cl_4$ (5). A solution of $CdCl_2$ (92 mg, 0.5 mmol) in 10 mL methanol was added dropwise to a solution of L_1^1 (100 mg, 0.5 mmol) in 5 mL methanol with stirring. The precipitate was filtered off and dried *in vacuo* (128.0 mg, 67%). Recrystallization from acetonitrile and toluene gave colorless X-ray quality crystals of **5**. The complex decomposed at 205 °C. Anal. Calcd for $C_{18}H_{26}Cd_2Cl_4N_2S_4$: C, 28.25; H, 3.42; N, 3.66. Found: C, 28.32; H, 3.39; N, 3.61. ^{1}H NMR (CD_3CN, 20 °C): 2.06 (s, 6H, H_g), 4.15 (s, 4H, H_f), 7.48 (d, 2H, J = 8 Hz, H_m), 7.96 (t, 1H, J = 8 Hz, H_p).

Preparation of $Zn(L_1^1)Cl_2$ (6). A solution of $ZnCl_2$ (68 mg, 0.5 mmol) in 5 mL acetone was added dropwise to a solution of L_1^1 (100 mg, 0.5 mmol) in 5 mL acetone with stirring. The solution was slowly diluted with 10 mL toluene and set aside for slow evaporation. Colorless X-ray quality crystals of **6** (109.0 mg, 65%) formed upon standing for 3 days. Mp: 198–199 °C. Anal. Calcd for $C_9H_{13}Cl_2NS_2Zn$: C, 32.21; H, 3.90; N, 4.17. Found: C, 32.30; H, 3.79; N, 4.19. ^{1}H NMR (2 mM, CD_3CN, 20 °C): 2.27 (s, 6H, H_g), 4.05 (s, 4H, H_f), 7.48 (d, 2H, J = 7 Hz, H_m), 7.96 (t, 1H, J = 7 Hz, H_p).

Preparation of $Pb(L_1^1)_2(ClO_4)_2$ (7). A solution of $Pb(ClO_4)_2{\cdot}3H_2O$ (230 mg, 0.5 mmol) in 5 mL acetonitrile was added dropwise a solution of L_1^1 (100 mg, 0.5 mmol) in 5 mL methanol with stirring . The mixture was slowly diluted with 6 mL 2-propanol and set aside for slow evaporation. Colorless X-ray quality crystal of **7** (76.7 mg, 36%) formed upon standing for 4 days. mp: 201–202 °C. Anal. Calc. for $C_{18}H_{26}Cl_2PbN_2O_8S_4$: C, 26.86; H, 3.26; N, 3.49. Found: C, 27.02; H, 3.33; N, 3.61. ^{1}H NMR (2 mM, CD_3CN, 20 °C): δ 2.19 (s, 6H, H_g), 4.19 (s, 4H, H_f), 7.47 (d, 2H, J = 8 Hz, H_m), 7.94 (t, 1H, J = 8 Hz, H_p).

Preparation of $Hg(L_2)_2(ClO_4)_2$ (8). A solution of $Hg(ClO_4)_2 \cdot 3H_2O$ (227 mg, 0.5 mmol) in 3 mL acetonitrile was added to a solution of L_2 (189 mg, 1.04 mmol) in 3 mL methanol with stirring. Colorless small crystals of **8** (48.0 mg, 13%) suitable for X-ray crystallography were obtained in 10 mm glass tubes after 6 days by slow diffusion of the mixture into benzene. Mp: 101–102 °C. Anal. Calcd for $C_{18}H_{28}Cl_2N_4O_8S_2Hg$: C, 28.29; H, 3.69; N, 7.33. Found: C, 28.18; H, 3.55; N, 7.33. ^{1}H NMR (2 mM, CD_3CN, –40 °C): 2.88 (broad, 2H), 3.40 (broad, 1H), 3.90 (broad, 1H), 4.14 (d, 1H, J = 16 Hz, H_f'), 4.26 (dd, 1H, J = 16, 4 Hz, H_f), 7.50 (t, 1H, J = 6 Hz, H_b), 7.58 (d, J = 8 Hz, 1 H, H_d), 8.00 (d, 1H, J = 5 Hz, $J(^{199}Hg^1H)$ = 18 Hz, H_a), 8.04 (t, 1H, J = 7 Hz, H_c), 8.43 (d, J = 5 Hz, «1H, $J(^{199}Hg^1H)$ = 12 Hz, H_a).

Preparation of $Cd(L_2)_2(ClO_4)_2 \cdot H_2O$ (9). A solution of $Cd(ClO_4)_2 \cdot 6H_2O$ (210 mg, 0.5 mmol) in 3 mL acetonitrile was added to a solution of L_2 (189 mg, 1.04 mmol) in 3 mL methanol with stirring. Colorless small crystals of **9** (71.4 mg, 21%) suitable for X-ray crystallography were obtained in 10 mm glass tubes after a week by slow diffusion of the mixture into toluene. Mp: 163–165 °C. Anal. Calcd for $C_{18}H_{30}Cl_2N_4O_9S_2Cd$: C, 31.15; H, 4.36; N, 8.08. Found: C, 31.26; H, 4.27; N, 8.07. ^{1}H NMR (2 mM, CD_3CN, –40 °C): 2.81 (broad, 2H), 3.26 (broad, 1H), 3.65 (broad, 1H), 4.03 (d, 1H, J = 16 Hz, $J(^{113}Cd^1H)$ = 27 Hz, H_f'), 4.25 (dd, 1H, J = 16, 5 Hz, $J(^{113}Cd^1H)$ = 17 Hz, H_f), 7.52 (t, 1H, J = 6 Hz, H_b), 7.61 (d, 1H, J = 8 Hz, H_d), 8.03 (d, 1H, J = 5 Hz, $J(^{113}Cd^1H)$ = 9 Hz, H_a), 8.08 (t, 1H, J = 8 Hz, H_c), 8.45 (d, J = 5 Hz, «1H, $J(^{113}Cd^1H)$ = 9 Hz, H_a).

Preparation of $Zn(L_2)_2(ClO_4)_2 \cdot H_2O$ (10). A solution of $Zn(ClO_4)_2 \cdot 6H_2O$ (186 mg, 0.5 mmol) in 3 mL acetonitrile was added to a solution of L_2 (189 mg, 1.04 mmol) in 3 mL methanol with stirring. Pink crystals of **10** (105.0 mg, 32%) suitable for X-ray

crystallography were obtained in 10 mm glass tubes after a week by slow diffusion of the mixture into benzene. Mp: 188–189 °C. Anal. Calcd for $C_{18}H_{30}Cl_2N_4O_9S_2Zn$: C, 33.42; H, 4.67; N, 8.66. Found: C, 33.41; H, 4.67; N, 8.80. ^{1}H NMR (2 mM, CD_3CN, –40 °C): 2.80 (broad, 1H), 3.26 (broad, 1H), 3.93 (broad, 1H), 4.02 (d, 1H, J = 17 Hz, H_f'), 4.23 (d, 1H, J = 17 Hz, H_f), 7.56 (t, 1H, J = 6 Hz, H_b), 7.63 (d, 1H, J = 8 Hz, H_d), 8.02 (broad, 1H, H_a), 8.13 (td, 1H, J = 8, 1 Hz, H_c), 8.40 (d, J = 5 Hz, «1H, H_a).

Preparation of $Zn(L_2)Cl_2$ (11). A solution of $ZnCl_2$ (68 mg, 0.5 mmol) in 3 mL acetonitrile was added to a solution of L_2 (95 mg, 0.52 mmol) in 3 mL methanol with stirring. Colorless small crystals of **11** (45.6 mg, 29%) suitable for X-ray crystallography were obtained in 10 mm glass tubes after a week by slow diffusion of the mixture into benzene. Mp: 157–158 °C. Anal. Calcd for $C_9H_{14}Cl_2N_2SZn$: C, 33.93; H, 4.43; N, 8.80. Found: C, 34.14; H, 4.59; N, 8.77. ^{1}H NMR (2 mM, CD_3CN, –40 °C): 2.80 (broad), 3.03 (broad), 3.85 (broad), 4.00 (broad), 4.29 (broad), 7.50 (d, 1H, J = 8 Hz, H_d), 7.57 (t, 1H, J = 7 Hz, H_b), 8.05 (td, 1H, J = 8, 2 Hz, H_c), 8.59 (d, 1H, J = 5 Hz, H_a).

Preparation of $[Hg_4(L_3)_4](ClO_4)_4$·6acetone (12). A solution of $Hg(ClO_4)_2·3H_2O$ (113 mg, 0.25 mmol) in 5 mL acetone was added dropwise to a solution of L_3 (60 mg, 0.25 mmol) in 5 mL acetone with stirring. The mixture was slowly diluted with benzene and set aside for slow evaporation after the precipitate was filtered off. Colorless X-ray quality crystal of **12** formed upon standing for 24 hrs. However, the crystals turned opaque when leaving the mother liquid. X-ray crystallography showed that the crystal contained three loosely held acetone molecules. Yield: 28%. mp: 159–160 °C. Anal. Calcd for $C_{44}H_{68}Cl_4N_8O_{16}S_8Hg_4$: C, 24.40; H, 3.16; N, 5.18. Found: C, 24.74; H, 3.21; N,

5.08. ^{1}H NMR (2 mM, CD_3CN, 20 °C): 2.73 (broad), 2.99 (broad), 3.33 (broad), 4.05 (broad), 7.43 (broad), 7.61 (broad), 8.08 (broad), 8.64 (broad), 8.81 (broad).

Preparation of $[Cd_3(L_3)_3(CO_3)](ClO_4)\cdot 0.5H_2O$ (13). A solution of $Cd(ClO_4)_2\cdot 6H_2O$ (105 mg, 0.25 mmol) in 5 mL acetone was added dropwise to a solution of $\mathbf{L_3}$ (60 mg, 0.25 mmol) in 5 mL acetone with stirring. The mixture was made slightly basic by adding 0.1 mL triethylamine and set aside for slow evaporation. Colorless X-ray quality crystal of **14** (48.6 mg, 47%) formed upon standing for 3 days. mp: 107–108 °C. Anal. Calc. for $C_{34}H_{52}Cd_3ClN_6O_{7.50}S_6$: C, 32.96; H, 4.31; N, 6.79. Found: C, 33.25; H, 4.22; N, 6.68. ^{1}H NMR (2 mM, CD_3CN, 20 °C): 2.49 (broad, 2H), 2.60 (broad, 1H), 2.76 (broad, 2H), 3.00 (broad, 1H), 3.24 (broad, 1H), 3.87 (d, 1H, J = 15 Hz, $J(^{113}Cd^1H)$ = 9 Hz), 4.01 (d, 1H, J = 15 Hz), 6.74 (t, 1H, J = 6 Hz), 7.35 (d, 1H, J = 8 Hz), 7.71 (td, 1H, J = 8, 2 Hz), 8.31 (broad, 1H).

RESULTS AND DISCUSSION

I. Crystal Structures of L_1^1–Containing Metal Complexes

$\mathbf{L_1^1}$ acts as a tridentate chelating ligand in the solid-state structures of complexes **1-7**. Complexes **1-3** consist of dications $[Hg(\mathbf{L_1^1})]^{2+}$, $[Cd(\mathbf{L_1^1})]^{2+}$ and $[Zn(\mathbf{L_1^1})]^{2+}$, respectively (Figures 3-5), and well-separated perchlorate anions. However, two oxygen donors from the perchlorate anions are found in the coordination sphere of complex **7** (Figure 6). The selected bond distances and angles for complexes **1-3** and **7** are given in Tables 9 and 11. Complexes **1-3** and **7** are the first crystallographically characterized complexes of this class of ligands with 1:2 metal-to-ligand ratios. The structures of chloride complexes $Hg(\mathbf{L_1^1})Cl_2$ (**4**), $[Cd(\mathbf{L_1^1})Cl_2]_2$ (**5**) and $Zn(\mathbf{L^1})Cl_2$ (**6**) are shown in Figure 7-9. Similar coordination spheres have been observed in $[Cu(\mathbf{L_1^8})Cl_2]$,[32] $[Cu(\mathbf{L_1^2})Cl_2]$,[34] $[Cu(\mathbf{L_1^3})Br]$, $[Ni(\mathbf{L_1^3})Br_2]$,[27] $[Cd(\mathbf{L_1^2})Cl(\mu\text{-}Cl)]_2$[33] and $[Zn(\mathbf{L_1^2})Br_2]$.[35] Selected bond distances and angles for complexes **4-6** are given in Tables 12 and 13.

Crystal Structure of $Hg(\mathbf{L_1^1})_2(ClO_4)_2$ (1). As shown in Figure 3, the $[Hg(\mathbf{L_1^1})]^{2+}$ cation has a meridional octahedral structure with crystallographically imposed C_2 symmetry and N-Hg-N bond angle of 174.7(2)°. The $\mathbf{L_1^1}$ ligands are rotated 73° relative to each other with intraligand S-Hg-S and average N-Hg-S bond angles of 149.16(5)° and 74.6(7)°, respectively. The thioether methyl groups of both ligands are arranged *trans* with respect to the pyridyl planes. The 2.406(5) Å Hg-N distance is similar to the Hg-$N_{pyridyl}$ distances observed in other six coordinate complexes such as $[Hg(pyridine)_6](CF_3SO_3)_2$ and $Hg(BMPA)_2(ClO_4)_2$ (BMPA = bis[(2-pyridyl)methyl]amine).[12,42] The Hg-S distances of 2.676(2) and 2.754(2) Å are close to those (2.654(1) and 2.671(1) Å) recently reported for $Hg(Py_2S)_2(ClO_4)_2$ (Py_2S = bis(2-methylpyridyl)sulfide)[14] and

comparable to those observed in six coordinate Hg(II) complexes of macrocyclic thioethers.[43,44] Each of the five-membered chelate rings in **1** adopts an envelope conformation with the S 1.0 Å from the plane containing Hg, N, and two lutidyl C. The Hg-O (perchlorate) distances (3.874-6.350 Å) are greater than the sum of van der Waal radii for Hg and O (r_{vdw}(Hg) = 1.70-2.00 Å, r_{vdw}(O) = 1.54 Å).[45]

The only other structurally characterized Hg(II) complex with a $N_2(SR_2)_4$ metal coordination sphere is the $Hg(PF_6)_2$ complex of 1,4,10,13-tetrathia-7,16-diazacyclo-octadecane (TDO).[46] This complex crystallized in a distorted octahedral coordination geometry. The average Hg-S distance for the four sulfur donors in the equatorial plane of the TDO complex was 2.695(5) Å, which is very similar to the equatorial plane of complex **1**. The aliphatic nitrogens in the axial positions had an Hg-N distance of 2.472(2) Å, slightly longer than Hg-$N_{pyridine}$ distance in **1.**

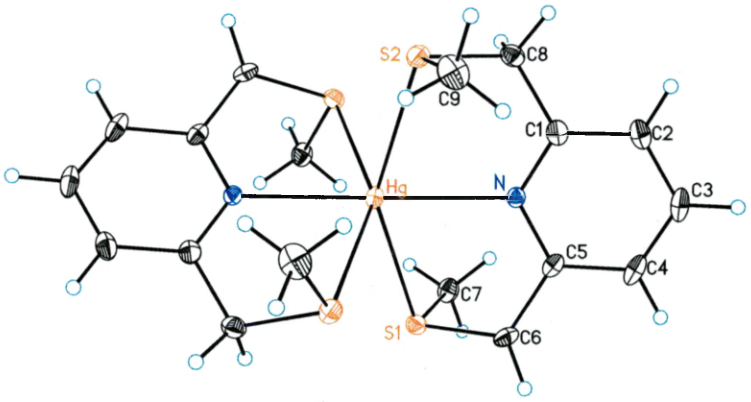

Figure 3. Structure of the cation of $Hg(\mathbf{L_1}^1)_2(ClO_4)_2$ (**1**). Thermal ellipsoids are shown at the 50% level. Anions are omitted for clarity.

Crystal Structure of $Cd(\mathbf{L_1}^1)_2(ClO_4)_2$ (2). Complex **2** crystallizes in the orthorhombic *Pcca* space group with eight formula units per cell. The unit cell contains two similar but crystallographically independent $[Cd(\mathbf{L_1}^1)_2]^{2+}$ cations (Figure 4). Both

meridional octahedral $[Cd(\mathbf{L_1}^1)]^{2+}$ cations have crystallographically imposed C_2 symmetry. The N-M-N bond angles of 175.05(7)° and 178.02(7)° in **2** are closer to linear than those in **1**. The $\mathbf{L_1}^1$ pyridyl planes are rotated 77° relative to each other. The average M-N (2.362(7) Å) and M-S (2.7153(3) Å) bond lengths of **2** are slightly shorter and nearly identical, respectively, to those in **1**. The thioether methyl groups of both ligands are arranged *trans* with respect to the pyridyl planes and the average intraligand S-M-S and N-M-S bond angles of 151.12(6)° and 75.591(5)° in **2** are similar to those observed in complex **1,** indicating the ligands are in a similar conformation. No other structurally characterized Cd(II) complex with a $N_2(SR_2)_4$ metal coordination sphere has been reported.

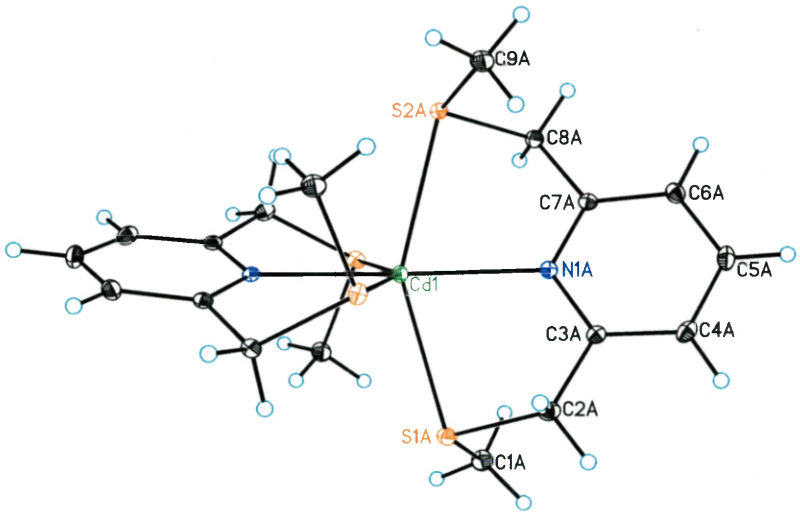

Figure 4. Structure of one of the two similar cations in the unit cell of $Cd(\mathbf{L_1}^1)_2(ClO_4)_2$ (**2**). Thermal ellipsoids are shown at the 50% level. Anions are omitted for clarity.

Crystal Structure of $Zn(\mathbf{L_1}^1)_2(ClO_4)_2$ (3). As shown in Figure 5, the $[Zn(\mathbf{L_1}^1)_2]^{2+}$ cation in complex **3** has a less distorted meridional octahedral structure than the cations of complexes **1** and **2**. Unlike **1** and **2** there is no crystallographically imposed symmetry

for **3**. The 175.23(9)° N-M-N bond angle in **3** is comparable to those observed in **1** and **2**. The $\mathbf{L_1}^1$ pyridyl planes are rotated 87° relative to each other. The two methyl groups in the thioether moieties are placed in a *trans* fashion with respect to the pyridyl rings as observed in complexes **1** and **2**. The Zn-$N_{pyridyl}$ distances of 2.119(3) and 2.125(3) Å are similar to those observed in six coordinate Zn(II) complexes[26,47-50] and also compare well with the Zn-N(His) distance in proteins,[11,51-54] but are significantly smaller than the M-N bond lengths in **1** and **2**. The Zn-S bond distances ranging from 2.530(1) to 2.651(1) Å are comparable to those in six-coordinate Zn(II) complexes,[22,55] but also significantly shorter than all the M-S bond lengths in **1** and **2**. The average intraligand S-M-S and N-M-S bond angles of 159.72(8) and 79.89(8)° in complex **3** are somewhat larger than those in complex **1** and **2** due to the shorter Zn-N bond lengths. No other structurally characterized Zn(II) complex with a $N_2(SR_2)_4$ metal coordination sphere has been reported.

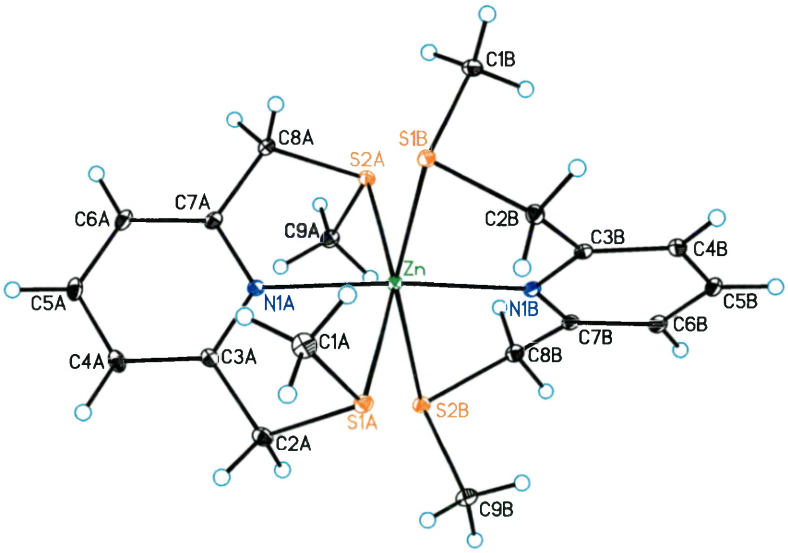

Figure 5. Structure of the cation of $Zn(\mathbf{L_1}^1)_2(ClO_4)_2$ (**3**). Thermal ellipsoids are shown at the 50% level. Anions are omitted for clarity.

Table 9. Selected bond distances (Å) and bond angles (deg) for complexes **1** and **2**

$Hg(\mathbf{L_1}^1)_2(ClO_4)_2$ (**1**)[a]		$Cd(\mathbf{L_1}^1)_2(ClO_4)_2$ (**2**)[b]	
Hg-N	2.406(5)	Cd(1)-N(1A)	2.3558(14)
Hg-S(1)	2.6763(16)	Cd(1)-S(1A)	2.7077(5)
Hg-S(2)	2.7538(17)	Cd(1)-S(2A)	2.7356(6)
		Cd(2)-N(1B)	2.3673(15)
		Cd(2)-S(1B)	2.6819(5)
		Cd(2)-S(2B)	2.7359(5)
N#1-Hg-N	174.7(2)	N(1A)#1-Cd(1)-N(1A)	178.02(7)
N-Hg-S(1)	75.28(13)	N(1A)#1-Cd(1)-S(1A)	105.57(4)
N-Hg-S(1)#1	107.95(12)	N(1A)-Cd(1)-S(1A)	75.69(4)
S(1)-Hg-S(1)#1	107.87(7)	S(1A)-Cd(1)-S(1A)#1	104.51(2)
N-Hg-S(2)#1	102.85(12)	N(1A)#1-Cd(1)-S(2A)	103.36(4)
S(1)-Hg-S(2)#1	81.20(5)	N(1A)-Cd(1)-S(2A)	75.41(4)
N-Hg-S(2)	73.88(13)	S(1A)-Cd(1)-S(2A)	151.077(14)
S(1)-Hg-S(2)	149.16(5)	S(1A)-Cd(1)-S(2A)#1	82.353(17)
S(2)#1-Hg-S(2)	106.37(8)	S(2A)-Cd(1)-S(2A)#1	105.37(2)
		N(1B)-Cd(2)-N(1B)#2	175.05(7)
		N(1B)-Cd(2)-S(1B)	76.10(4)
		N(1B)-Cd(2)-S(1B)#2	106.99(4)
		S(1B)-Cd(2)-S(1B)#2	106.28(2)
		N(1B)-Cd(2)-S(2B)	75.15(4)
		S(1B)-Cd(2)-S(2B)	151.168(14)
		N(1B)-Cd(2)-S(2B)#2	101.84(4)
		S(1B)-Cd(2)-S(2B)#2	80.299(17)
		S(2B)-Cd(2)-S(2B)#2	107.72(2)

[a]Symmetry transformations used to generate equivalent atoms: -x, -y+1/2, z; x, -y+1, -z+1/2; -x-1/2, y, -z.
[b]Symmetry transformations used to generate equivalent atoms: -x+3/2, -y+1, z; -x+1/2, y, z; -x+1, y, -z+3/2; -x+2, y, -z+3/2

Comparisons of complexes 1–3 to related complexes of physiologically essential metal ions. Although no metal complexes of $\mathbf{L_1}$-type ligands with a 1:2 metal-to-ligand ratio have been previously structurally characterized, there are a handful of structurally characterized complexes of the physiologically essential divalent metal ions with $N_2(SR_2)_4$ coordination spheres. The metal complexes of type $M[N_2(SR_2)_4]^{2+}$ (M = Cu(II),[56-58] Ni(II),[59-64] Co(II),[65] Co(III),[62] and Fe(II)[66,67]) with noncoordinating counterions all possess a distorted meridional C_{2v} or trans facial D_{2h} coordination geometry. Table 10 indicates the range of M-N and M-S bond lengths observed in these

complexes. The Cu-$N_{aliphatic}$ bond has the largest range of 2.01(1) to 2.19(2) Å, and all other first row transition metal bond distances M-$N_{aliphatic}$ fall into this range. As might be expected, the average for M-N bond distances increases as one moves down the group 12 family (Zn-N < Cd-N < Hg-N) consistent with the increased metal ion radius. Inspection of Table 10 also indicates that the range of M(II)-S bond distances follow the nearly periodic trend Fe < Ni < Co < Cu < Zn for the first row transition metal ions. While the group 12 metal ions present the feature Zn-S < Cd-S ~ Hg-S, which was also observed in the six coordinate group 12 metal crown thioether complexes $[M(10S3)_2](ClO_4)_2 \cdot 2CH_3NO_3$ (10S3 = bis(1,4,7-trithiacyclodecane).[55]

Table 10. Comparison of M-N, M-N and M-S bond length (Å) ranges for known complexes with $N_2(SR_2)_4$ coordination spheres.

Metal Ion	M-$N_{aliphatic}$ (Å)	M-$N_{aromatic}$ (Å)	M-S (Å)	Reference
Fe(II)	2.022(4) – 2.038		2.248(1) – 2.2674(15)	66,67
Co(II)		2.100(3)	2.460(1) – 2.486(1)	65
Co(III)	1.9993(4), 1.994(4)		2.249(1) – 2.268(1)	62
Ni(II)	2.065(13) – 2.126(13)	2.053(2) – 2.091(5)	2.389(2) - 2.440(2)	59-64
Cu(II)	2.007(13) - 2.191(17)		2.487(5) - 2.578(5)	56-58
Zn(II)		2.119(3) - 2.125(3)	2.5300(11) - 2.6508(14)	This work
Cd(II)		2.3558(14) - 2.3673(15)	2.6819(5) - 2.7359(5)	This work
Hg(II)	2.472(17), 2.473(11)	2.406(5)	2.6764(17) - 2.7538(17)	This work, 46

Crystal Structure of $Pb(L_1^1)_2(ClO_4)_2$ (7). As shown in Figure 6, the 1:2 metal-to-L_1^1 complex of $Pb(ClO_4)_2$ is eight coordinate with a distorted dodecahedral geometry. In complex **7**, two oxygen donors of the perchlorate anions and three donor groups from each of two ligands are bound to Pb(II). The average Pb-N and Pb-O bond lengths are

2.733(4) and 2.920(4) Å, respectively. The Pb(II)-S bonds consist of two shorter (2.8606(11) and 2.8646(11) Å) and two longer (3.1817(11) and 3.1829(12) Å) distances. These distances are larger than those observed in complexes **1-3** as expected for a higher coordination number complex. The interligand M-N-M bond angle of 131.31(11)° is much smaller that those in complexes **1-3** due to the coordination of the perchlorate anions. The average intraligand S-M-S and N-M-S bond angles of 130.27(3)° and 65.80(8)° in complex **7** are also smaller than those in complex **1-3**. The two thioether methyl groups of both ligands are arranged *trans* with respect to the pyridyl planes closely resembling complexes **1-3**. The above results suggest that Pb(II) has a higher affinity for oxygen donors in comparison to the divalent group 12 metal ions. Moreover, coordination of the counter ion has an important effect on the ligand conformation and the geometry of the central metal ions.

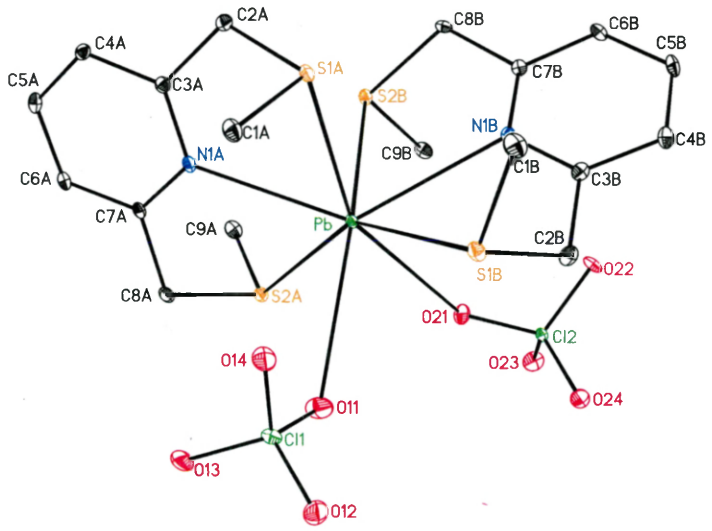

Figure 6. Structure of $Pb(\mathbf{L_1}^1)_2(ClO_4)_2$ (**7**). Thermal ellipsoids are shown at the 50% level.

Table 11. Selected bond distances (Å) and bond angles (deg) for complexes **3** and **7**

$Zn(\mathbf{L_1}^1)_2(ClO_4)_2$ (**3**)[a]		$Pb(\mathbf{L_1}^1)_2(ClO_4)_2$ (**7**)	
Zn-N(1B)	2.119(3)	Pb- N(1A)	2.720(4)
Zn-N(1A)	2.125(3)	Pb- N(1B)	2.746(4)
Zn-S(1B)	2.5300(11)	Pb- S(1A)	2.8606(11)
Zn-S(2A)	2.5519(13)	Pb- S(2B)	2.8646(11)
Zn-S(1A)	2.5730(14)	Pb- O(21)	2.878(4)
Zn-S(2B)	2.6508(14)	Pb- O(11)	2.962(4)
		Pb -S(2A)	3.1817(11)
		Pb -S(1B)	3.1829(12)
N(1B)-Zn-N(1A)	175.23(9)	N(1A)-Pb-N(1B)	131.31(11)
N(1B)-Zn-S(1B)	81.41(8)	N(1A)-Pb-S(1A)	66.96(9)
N(1A)-Zn-S(1B)	102.76(8)	N(1B)-Pb-S(1A)	79.06(8)
N(1B)-Zn-S(2A)	102.19(8)	N(1A)-Pb-S(2B)	75.61(8)
N(1A)-Zn-S(2A)	80.06(8)	N(1B)-Pb-S(2B)	66.81(8)
S(1B)-Zn-S(2A)	92.83(4)	S(1A)-Pb-S(2B)	84.01(3)
N(1B)-Zn-S(1A)	98.10(7)	N(1A)-Pb-O(21)	134.23(12)
N(1A)-Zn-S(1A)	79.56(7)	N(1B)-Pb-O(21)	74.60(11)
S(1B)-Zn-S(1A)	92.15(4)	S(1A)-Pb-O(21)	153.61(9)
S(2A)-Zn-S(1A)	159.61(3)	S(2B)-Pb-O(21)	87.16(9)
N(1B)-Zn-S(2B)	78.53(8)	N(1A)-Pb-O(11)	99128.63(13).
N(1A)-Zn-S(2B)	97.20(8)	N(1B)-Pb-O(11)	97(13)
S(1B)-Zn-S(2B)	159.84(3)	S(1A)-Pb-O(11)	133.94(8)
S(2A)-Zn-S(2B)	93.39(4)	S(2B)-Pb-O(11)	137.57(9)
		O(21)-Pb-O(11)	65.57(11)
		N(1A)-Pb-S(2A)	65.79(9)
		N(1B)-Pb-S(2A)	129.50(8)
		S(1A)-Pb-S(2A)	132.09(3)
		S(2B)-Pb-S(2A)	77.26(3)
		O(21)-Pb-S(2A)	69.17(9)
		O(11)-Pb-S(2A)	63.20(10)
		N(1A)-Pb-S(1B)	131.07(9)
		N(1B)-Pb-S(1B)	63.64(8)
		S(1A)-Pb-S(1B)	73.78(3)
		S(2B)-Pb-S(1B)	128.45(3)
		O(21)-Pb-S(1B)	92.80(9)
		O(11)-Pb-S(1B)	86.69(10)
		S(2A)-Pb-S(1B)	149.05(3)

[a] Symmetry transformations used to generate equivalent atoms: x-1/2, -y+1/2, z-1/2; -x+1, -y,-z

Crystal Structure of $Hg(\mathbf{L_1}^1)Cl_2$ (4). As shown in Figure 7, complex **4** has a nearly tetragonal Hg(II) coordination geometry (τ = 0.06).[68] The largest angles between atoms in the basal plane of the complex are 142.7(1)° for S(1)-Hg-S(2) and 139.3(2)° for

Cl(1)-Hg-Cl(2). Five-coordinate Hg(II) complexes exhibiting similar trigonal bipyramid distortions are known.[7,69,70] With $\mathbf{L_1}$-type ligands, distorted trigonal bipyramid geometries have also been observed in complexes [Cu($\mathbf{L_1}^8$)Cl_2] and [Zn($\mathbf{L_1}^2$)Br_2.[32,35]However, a distorted square pyramidal geometry is observed in [Ni($\mathbf{L_1}^3$)Br_2] and [Cu($\mathbf{L_1}^2$)Cl_2], with the nitrogen, two sulfur and one halide atoms occupying the four basal positions of the square pyramid.[27]

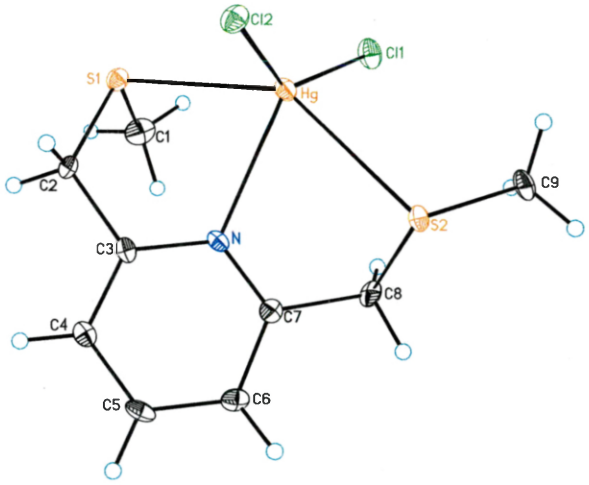

Figure 7. Structure of Hg($\mathbf{L_1}^1$)Cl_2 (**4**). Thermal ellipsoids are shown at the 50% level.

Inspection of Tables 9 and 12 shows that the 2.454(1) Å Hg-N and 2.8162(7) Å average Hg-S bond lengths in **4** are essentially identical and only 0.101(5) Å longer, respectively, than their counterparts in complex **1.** The intraligand S-Hg-S and N-Hg-S bond angles of 142.7(1)° and 71.4(3)° are ~4.5% smaller than those in complex **1**. The most distinct difference between the ligand conformations in **4** and **1** is the *cis* and *trans* orientation, respectively, of the two methyl groups bonded to the two sulfur atoms. The Hg-Cl distances of 2.383(7) and 2.409(6) Å are comparable to the observed range of 2.310-2.428 Å in five coordinate complexes.[69-72]

Table 12. Selected bond distances (Å) and bond angles (deg) for complexes **4 and 5**

$Hg(\mathbf{L_1}^1)Cl_2$ (**4**)		$[Cd(\mathbf{L_1}^1)Cl_2]_2$ (**5**)	
Hg-Cl(1)	2.383(7)	Cd(1)-N(1A)	2.395(4)
Hg-Cl(2)	2.409(6)	Cd(1)-Cl(2A)	2.5301(12)
Hg-N	2.454(11)	Cd(1)-Cl(1A)	2.5355(11)
Hg-S(1)	2.777(7)	Cd(1)-Cl(2B)	2.7050(11)
Hg-S(2)	2.854(7)	Cd(1)-S(1A)	2.7060(12)
		Cd(1)-S(2A)	2.7342(12)
		Cd(2)-N(1B)	2.356(4)
		Cd(2)-Cl(1B)	2.5192(13)
		Cd(2)-Cl(2B)	2.5279(11)
		Cd(2)-S(1B)	2.7080(13)
		Cd(2)-S(2B)	2.7359(12)
		Cd(2)-Cl(2A)	2.7477(12)
Cl(1)-Hg-Cl(2)	139.31(17)	N(1A)-Cd(1)-Cl(2A)	168.48(9)
Cl(1)-Hg-N	116.7(3)	N(1A)-Cd(1)-Cl(1A)	93.51(10)
Cl(2)-Hg-N	103.9(3)	Cl(2A)-Cd(1)-Cl(1A)	97.43(4)
Cl(1)-Hg-S(1)	101.97(13)	N(1A)-Cd(1)-Cl(2B)	84.45(10)
Cl(2)-Hg-S(1)	93.20(16)	Cl(2A)-Cd(1)-Cl(2B)	84.48(4
N-Hg-S(1)	71.3(3)	Cl(1A)-Cd(1)-Cl(2B)	177.01(4)
Cl(1)-Hg-S(2)	94.89(15)	N(1A)-Cd(1)-S(1A)	73.09(10)
Cl(2)-Hg-S(2)	95.27(18)	Cl(2A)-Cd(1)-S(1A)	109.93(4)
N-Hg-S(2)	71.4(3)	Cl(1A)-Cd(1)-S(1A)	92.26(4)
S(1)-Hg-S(2)	142.70(10)	Cl(2B)-Cd(1)-S(1A)	89.23(4)
C(1)-S(1)-C(2)	101.7(8)	N(1A)-Cd(1)-S(2A)	73.79(9)
C(1)-S(1)-Hg	101.9(6)	Cl(2A)-Cd(1)-S(2A)	103.11(4)
C(2)-S(1)-Hg	94.0(5)	Cl(1A)-Cd(1)-S(2A)	86.93(4)
		Cl(2B)-Cd(1)-S(2A)	90.40(4)
		S(1A)-Cd(1)-S(2A)	146.76(4)
		N(1B)-Cd(2)-Cl(1B)	91.26(10)
		N(1B)-Cd(2)-Cl(2B)	169.95(9)
		Cl(1B)-Cd(2)-Cl(2B)	97.33(4)
		N(1B)-Cd(2)-S(1B)	76.62(10)
		Cl(1B)-Cd(2)-S(1B)	101.50(4)
		Cl(2B)-Cd(2)-S(1B)	106.56(4)
		N(1B)-Cd(2)-S(2B)	74.00(9)
		Cl(1B)-Cd(2)-S(2B)	88. 98(4)
		Cl(2B)-Cd(2)-S(2B)	100.84(4)
		S(1B)-Cd(2)-S(2B)	148.98(4)
		N(1B)-Cd(2)-Cl(2A)	87.66(10)
		Cl(1B)-Cd(2)-Cl(2A)	178.38(4)
		Cl(2B)-Cd(2)-Cl(2A)	83.64(4)
		S(1B)-Cd(2)-Cl(2A)	79.43(4)
		S(2B)-Cd(2)-Cl(2A)	89.56(4)
		Cd(1)-Cl(2A)-Cd(2)	95.02(4)
		Cd(2)-Cl(2B)-Cd(1)	96.13(4)

Crystal Structure of $[Cd(L_1^1)Cl(\mu\text{-}Cl)]_2$ (5). Complex **5** exists in the solid-state as a dimer asymmetrically bridged by two chloride ligands (Figure 8). Each of the Cd(II) centers adopts a distorted octahedral geometry with one tridentate L_1^1 ligand, two bridging chlorides and one terminal chloride atom occupying the six positions. The ligand L_1^1 is bound to Cd(II) in an approximately meridional fashion with one bridging chloride atom in the same plane, and the terminal and the other bridging chloride ligand in the axial positions. It is interesting to note that the two L_1^1 are arranged in different configurations. In the dimer, the two methyl groups of one L_1^1 ligand are found *cis* about the pyridyl plane but those of the other ligand are *trans*, resembling $Hg(L_1^1)Cl_2$ and $Zn(L_1^1)Cl_2$, respectively (see the following section for $Zn(L_1^1)Cl_2$). Moreover, the dimeric structure of complex **5** indicates the greater tendency of Cd(II) for octahedral coordination relative to Hg(II) and Zn(II) and the flexible ligation capacity of halide ligands.[73] A similar dimeric structure was observed in complex $[Cd(L_1^2)Cl(\mu\text{-}Cl)]_2$.[33]

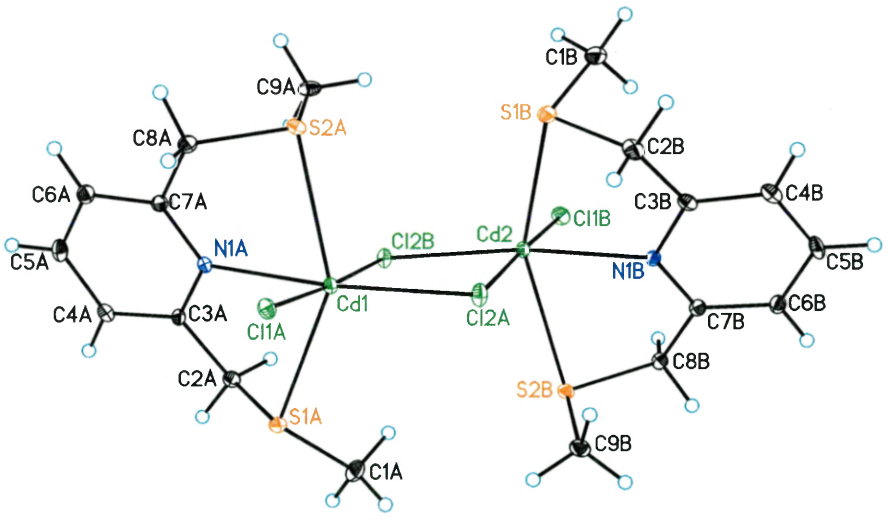

Figure 8. Structure of $[Cd(L_1^1)Cl(\mu\text{-}Cl)]_2$ (**5**). Thermal ellipsoids are shown at the 50% level.

The average Cd-Cl_{bridge} bond distance of 2.6276(87) Å and Cd-Cd distance of 3.894 Å are comparable to those in chloride bridged Cd(II) dimers and polymers.[74,75] The average Cd-$Cl_{terminal}$ bond distance is 2.527(6) Å, similar to those found in six coordinate Cl-bridged Cd(II) complexes.[29,75] The average Cd-S distance of 2.721(4) Å and Cd-N distance of 2.375(9) Å are close to 2.713(6) and 2.3803 Å observed in complex $[Cd(\mathbf{L_1}^2)Cl(\mu\text{-}Cl)]_2$, respectively.[33] The intraligand N-Cd-S bond angles range from 73.09(1)° to 76.62(10)°. The axial Cl_{bridge}-Cd-$Cl_{terminal}$ bond angles of 177.01(4)° and 178.38(4)° are slightly smaller than the ideal for an octahedral geometry.

Crystal Structure of $Zn(\mathbf{L_1}^1)Cl_2$ (6). Complex **6** contains two similar but crystallographically independent Zn(II) centers (Figure 9) in the crystal structure. Each Zn(II) ion is located in a coordination environment consisting of one tridentate $\mathbf{L_1}^1$ and two chloride ligands with slightly more trigonal bypyramidal character than tetragonal (τ = 0.525 [Zn(1)], 0.604 [Zn(2)]). The Zn, N, Cl(1), Cl(2) are coplanar, defining the equatorial plane, and the two sulfur atoms occupy axial positions. The structure closely resembles that of $Hg(\mathbf{L_1}^1)Cl_2$ except for the *trans* conformation of the two methyl groups with respect to the pyridine plane and a pseudo-C_2 axis along the Zn-N bond**.** The S-Zn-S bond angles of 161.10(2)° and 159.08(2)° deviate significantly from linearity. However, the angles between the atoms in the equatorial plane are approximately ideal ranging from 113.15(4)° to 129.62(2)°. The average Zn-S bond distance of 2.388(6) Å and Zn-N bond length of 2.15(1) Å are typical for the five-coordinate Zn(II) complexes[76,77] and comparable to Zn-S(Cys) and Zn-N(His) distances in proteins, respectively.[11,51-54,78-80] Teixidor et al.[35] previously reported a structurally similar complex $[Zn(\mathbf{L_1}^2)Br_2]$, which has ~12.5% larger Zn-S bond distances but comparable Zn-N distance. The R-groups in

complex [Zn($\mathbf{L_1}^2$)Br_2] were found *trans* to each other as observed in **6**. The intraligand S-Zn-S bond angle of 157.0(1)° and N-Zn-S of 78.5(7)° also compare well with those in **6**.

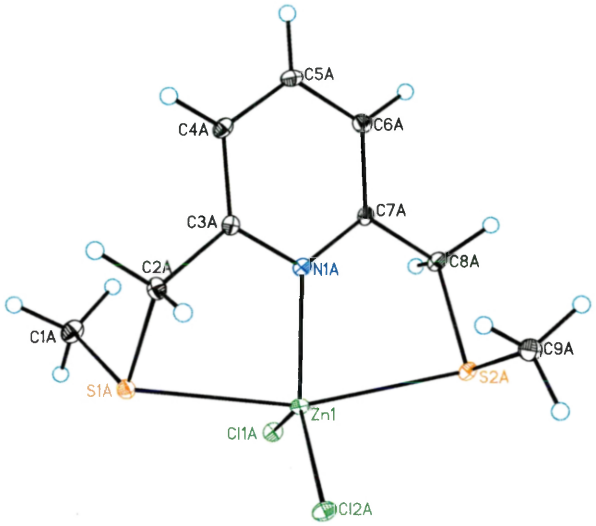

Figure 9. Structure of one of the two similar complexes in the unit cell of Zn($\mathbf{L_1}^1$)Cl_2 (**6**). Thermal ellipsoids are shown at the 50% level.

Table 13. Selected bond distances (Å) and bond angles (deg) for complex **6**

Bond Distances		Bond Angles	
Zn(1)-N(1A)	2.0785(15)	N(1A)-Zn(1)-Cl(2A)	117.21(4)
Zn(1)-Cl(2A)	2.2333(8)	N(1A)-Zn(1)-Cl(1A)	113.15(4)
Zn(1)-Cl(1A)	2.5741(9)	Cl(2A)-Zn(1)-Cl(1A)	129.62(2)
Zn(1)-S(1A)	2.5814(9)	N(1A)-Zn(1)-S(1A)	81.78(4)
Zn(1)-S(2A)	2.0828(15)	Cl(2A)-Zn(1)-S(1A)	88.89(3)
Zn(2)-N(1B)	2.2190(8)	Cl(1A)-Zn(1)-S(1A)	97.09(3)
Zn(2)-Cl(1B)	2.2326(8)	N(1A)-Zn(1)-S(2A)	79.79(4)
Zn(2)-Cl(2B)	2.6168(9)	Cl(2A)-Zn(1)-S(2A)	95.82(2)
Zn(2)-S(1B)	2.6318(8)	Cl(1A)-Zn(1)-S(2A)	93.96(3)
Zn(2)-S(2B)	2.2548(7)	S(1A)-Zn(1)-S(2A)	161.101(16)
		N(1B)-Zn(2)-Cl(1B)	119.52(5)
		N(1B)-Zn(2)-Cl(2B)	117.61(4)
		Cl(1B)-Zn(2)-Cl(2B)	122.87(2)
		N(1B)-Zn(2)-S(1B)	79.12(5)
		Cl(1B)-Zn(2)-S(1B)	98.68(2)
		Cl(2B)-Zn(2)-S(1B)	92.08(3)
		N(1B)-Zn(2)-S(2B)	79.96(5)
		Cl(1B)-Zn(2)-S(2B)	91.63(3)
		Cl(2B)-Zn(2)-S(2B)	97.55(3)
		S(1B)-Zn(2)-S(2B)	159.083(18)

Symmetry transformations used to generate equivalent atoms: -x+3/2, -y+1, z+1/2; -x+3/2,-y,z-1/2; x+1/2, -y+1/2,- z; -x+3/2, -y+1, z-1/2

Comparisons of complexes 4-6 to related complexes of physiologically essential metal ions. The crystal structures of $[Cu(\mathbf{L_1}^8)Cl_2]$,[32] $[Cu(\mathbf{L_1}^2)Cl_2]$,[34] $[Cu(DAHT)Cl_2]$ (DAHT = 3,10-dithia-16-azabicyclo[10.3.1] hexadeca-1(16),12,14-triene),[34] $[Ni(\mathbf{L_1}^3)Br_2]$,[27] $[Ni(\mathbf{L_1}^3)Br(\mu\text{-}Br)]_2$,[28] have been previously reported. Complexes $[Cu(\mathbf{L_1}^2)Cl_2]$ and $[Cu(DAHT)Cl_2]$ exist in the solid state as monomers adopting distorted square pyramidal coordination geometries with the two thioether sulfur atoms, pyridine nitrogen and one chloride ion in a plane. $[Cu(\mathbf{L_1}^8)Cl_2]$ resembles complex **6** with a distorted trigonal bipyramidal geometry.[32] The Cu-S bond distances range from 2.338(3) to 2.431(1) Å with an average of 2.366(7) Å, which are shorter than Zn-S distances observed in complex **6**. The average Cu-N distance of 2.045(6) Å is comparable to the average Zn-N distance of 2.080(7) Å in complex **6**. The average S-Cu-S bond angles of 158.7(8)° is also comparable to the average Zn-S-Zn bond angle of 160.09(2)° observed in complex **6**.

The R-groups of the ligands in complexes $[Cu(\mathbf{L_1}^2)Cl_2]$[34] and $[Cu(\mathbf{L_1}^8)Cl_2]$[32] are both arranged in *trans* fashion as observed in complex **6**. The complex $[Ni(\mathbf{L}^3)Br_2]$[27] has a distorted square pyramidal geometry similar to $[Cu(\mathbf{L_1}^2)Cl_2]$. The average Ni(II)-S distance of 2.383(7) Å and Ni(II)-N distance of 2.057(5) Å compare well with the above Cu(II) complexes. However, a *cis* arrangement of the R-groups of the ligand was observed as in complex **4**. The dimeric complex $[Ni(\mathbf{L_1}^3)Br(\mu\text{-}Br)]_2$ has a distorted octahedral coordination geometry for Ni(II), which is similar to **5** and $[Cd(\mathbf{L_1}^2)Cl(\mu\text{-}Cl)]_2$.[28] The average Ni-N and Ni-S bond distances are 2.0557(5) and 2.443(7) Å, respectively. The R-groups are both *trans* to each other.

Crystallographic database searches revealed four other Cu(II)[81-84] and one Zn(II)[85] complexes with a $N(SR_2)_2X_2$ coordination sphere. Cu-S bond distances range from 2.313(2) to 2.369(2) Å with an average of 2.334(9) Å, which falls within the range reported above for Cu(II) complexes of $\mathbf{L_1}$-type ligands. The average Cu-$N_{pyridine}$ and Cu-$N_{aliphatic}$ bond distances are 2.025(9) and 2.174(4) Å, respectively. The average Zn-S and Zn-N bond distances are 2.618(1) and 2.080(3) Å, which are comparable to 2.686(7) and 2.083(5) Å, respectively, observed in $[Zn(\mathbf{L_1}^2)Br_2]$.

From the above discussion, the metal ions used to study the coordination chemistry of the $\mathbf{L_1}$-type ligands are limited to Cu(II) and Ni(II) with only a few cases of the heavy metals. Also, with only a few exceptions, this ligand is found coordinated to metal ions in a tridentate fashion. The mononuclear complexes $M[N(SR)_2X_2]$ with tridentate coordination all adopt a distorted square pyramidal or trigonal bipyramidal coordination geometry. The halide counterions are found in the primary coordination sphere, which could prevent a second ligand from binding the metal ions.

II. Crystal Structures of L^2-Containing Metal Complexes

In the solid-state $\mathbf{L_2}$ exhibits a tridentate binding mode in the crystal structures of complexes **8-11.** Similar to complexes **1-3**, complexes **8-10** consist of dications $[Hg(\mathbf{L_2})_2]^{2+}$, $[Cd(\mathbf{L_2})_2]^{2+}$ and $[Zn(\mathbf{L_2})_2]^{2+}$, respectively (Figures 10-12), and well-separated perchlorate anions. The selected bond distances and angles for complexes **8-10** are given in Tables 14. The chloride complexes $Hg(\mathbf{L_2})Cl_2$ and $Cd(\mathbf{L_2})Cl_2$[36] have been previously synthesized in our group, so $Zn(\mathbf{L_2})Cl_2$ (**11**) was prepared for comparison. As observed for the chloride metal complexes of $\mathbf{L_1}^1$, the zinc triad chloride complexes of $\mathbf{L_2}$ are nonhomologous. Complexes $Hg(\mathbf{L_2})Cl_2$ and $Zn(\mathbf{L_2})Cl_2$ are mononuclear, whereas

$Cd(\mathbf{L_2})Cl_2$ exists in the solid-state as a polymer. The selected bond distances and angles for complex **11** are given in Table 15.

Very similar structural features are present in all three $[M(\mathbf{L_2})_2]^{2+}$ cations. As shown in Figures 10-12, these cations adopt a trans facial octahedral geometry with the metal ion at the inversion center. Each ligand binds the metal ion to form two five-membered rings, one with the alkylamino nitrogen and the other with the ethylene carbon occupying the apex positions. Moreover, each pair of the five-membered rings defined by the same atoms from the two ligands is coplanar except the apex position. The two pyridyl rings are also coplanar. The interligand bond angles of N_{alkyl}-M-N_{alkyl}, $N_{pyridyl}$-M-$N_{pyridyl}$, and S-M-S are all 180°.

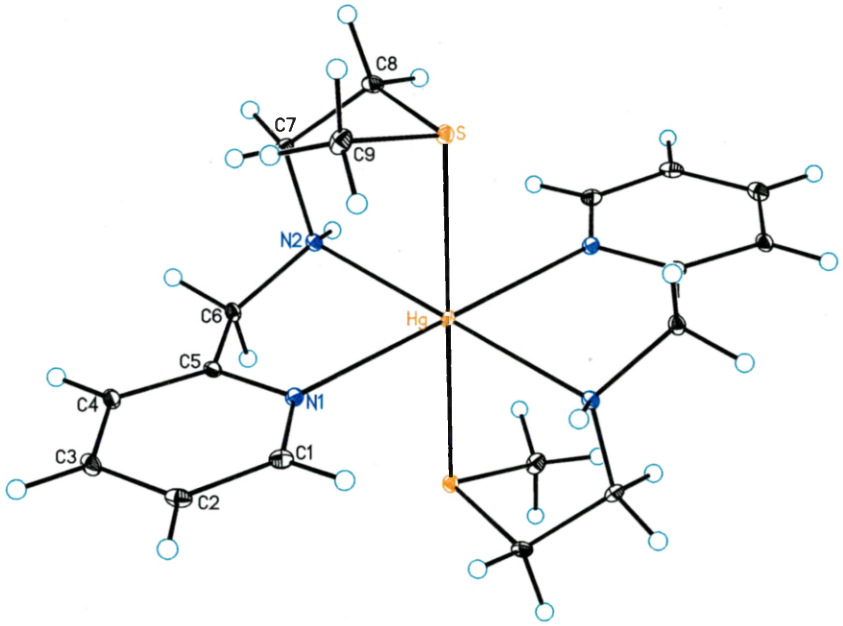

Figure 10. Structure of the cation of $Hg(\mathbf{L_2})_2(ClO_4)_2$ (**8**). Thermal ellipsoids are shown at the 50% level.

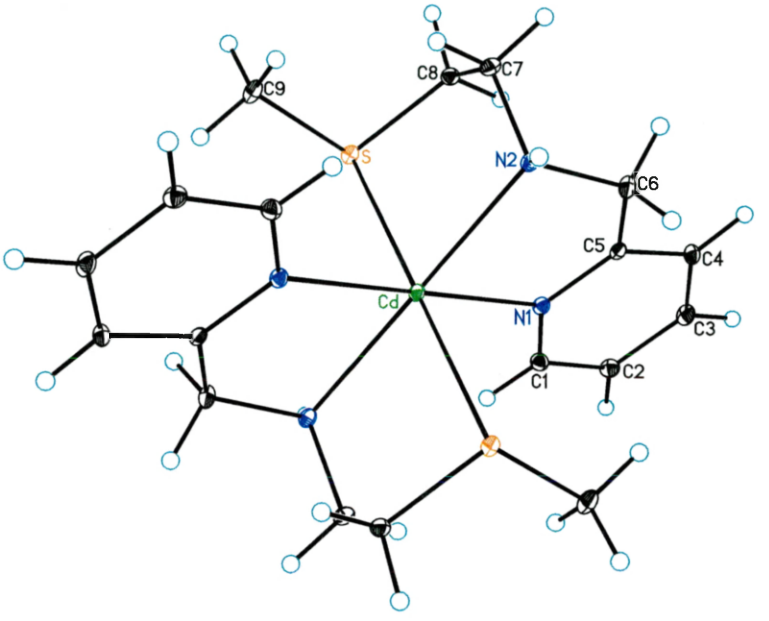

Figure 11. Structure of the cation of $Cd(\mathbf{L_2})_2(ClO_4)_2 \cdot H_2O$ (**9**). Thermal ellipsoids are shown at the 50% level.

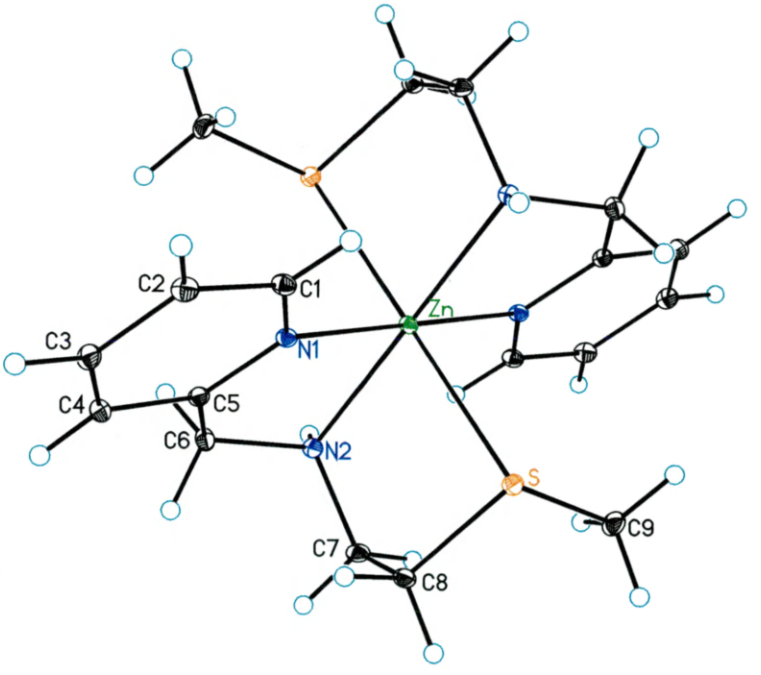

Figure 12. Structure of the cation of $Zn(\mathbf{L_2})_2(ClO_4)_2 \cdot H_2O$ (**10**). Thermal ellipsoids are shown at the 50% level.

Table 14. Selected bond distances (Å) and bond angles (deg) for complexes **8-10**

	$Hg(\mathbf{L_2})_2(ClO_4)_2$ (**8**)[a]	$Cd(\mathbf{L_2})_2(ClO_4)_2 \cdot H_2O$ (**9**)[b]	$Zn(\mathbf{L_2})_2(ClO_4)_2 \cdot H_2O$ (**10**)[c]
M-N(1)	2.424(2)	2.3133(17)	2.1059(19)
M-N(2)	2.305(2)	2.3826(17)	2.1773(17)
M-S	2.7989(13)	2.7115(7)	2.5978(13)
N(2)-M-N(2)#1	180.0	180.0	180.0
N(2)-M-N(1)	73.26(8)	74.38(5)	79.80(5)
N(2)-M-N(1)#1	106.75(8)	105.62(5)	100.20(5)
N(2)-M-S#1	99.59(7)	99.76(4)	95.85(5)
N(2)-M-S	80.41(7)	80.24(4)	84.15(5)
N(1)-M-S	95.51(6)	87.84(5)	88.13(7)
N(1)-M-N(1)#1	180.0	180.0	179.999(1)
N(1)-M-S#1	84.49(6)	92.16(5)	91.87(7)
S-M-S#1	180.0	180.0	180.0

[a]Symmetry transformations used to generate equivalent atoms: -x, -y+2, -z
[b]Symmetry transformations used to generate equivalent atoms: -x, -y+2, -z+2
[c]Symmetry transformations used to generate equivalent atoms: -x, -y+2, -z-1

Crystal Structure of $Hg(\mathbf{L_2})_2(ClO_4)_2$ (8). Complex **8** contains a $[Hg(\mathbf{L_2})_2]^{2+}$ cation (Figure 10) and two perchlorate anions. In $[Hg(\mathbf{L_2})_2]^{2+}$, the intraligand S-Hg-$N_{alkyl}$ S-Hg-$N_{pyridine}$ and N-Hg-N bond angles are 80.41(7)°, 95.51(6)° and 73.26(8)°, respectively. The interligand S-Hg-N_{alkyl}, S-Hg-$N_{pyridyl}$ and N_{alkyl}-Hg-$N_{pyridyl}$ bond angles are 99.50(7)°, 84.49(6)° and 106.75(8)°, respectively. The 2.424(2) Å Hg-$N_{pyridyl}$ distance is comparable to those observed in **1** and other six coordinate Hg(II) complexes.[12,42] The 2.305(2) Å Hg-N_{alkyl} distance is obviously shorter than the range of 2.40(1) to 2.473(11) Å observed in the six coordinate complexes $[Hg(TATC)](ClO_4)_2 \cdot 0.5H_2O$ (TATC = 1,4,7-tris(o-aminobenzyl)-1,4,7-triazacyclononane)[86] and $Hg(TDO)(PF_6)_2$.[46] In contrast, the Hg-S bond distance of 2.7989(13) Å is longer than the previously reported range of 2.458 to 2.751 Å for six coordinate Hg(II) complexes of thioethers.[14]

Crystal Structure of $Cd(\mathbf{L_2})_2(ClO_4)_2 \cdot H_2O$ (9). Complex **9** consists of a $[Cd(\mathbf{L_2})_2]^{2+}$ cation (Figure 11), two perchlorate anions and a non-coordinated water

molecule. Inspection of Tables 14 indicates that the ligand adopts a similar conformation in complexes **8** and **9**. The intraligand S-M-N_{alkyl} and N-M-N bond angles are only slightly smaller in complex **9** than in complex **8**. The interligand S-M-N_{alkyl} and N_{alkyl}-M-$N_{pyridyl}$ are nearly identical in complexes **9** and **8**. In contrast, the intraligand S-M-$N_{pyridyl}$ and interligand S-M-$N_{pyridyl}$ bond angles are substantially bigger and smaller, respectively, in complex **9** than in complex **8**. The Cd-$N_{pyridyl}$ distance of 2.3132(17) Å is comparable to those (2.266-2.442 Å) found in pyridine-containing six-coordinate Cd(II) complexes.[14] The Cd-N_{alkyl} distance of 2.3826(17) Å resembles those found in the six coordinate complex $[Cd(TATC)](ClO_4)_2 \cdot 0.5H_2O$.[86] This distance is slightly longer than that found in complex **8.** The Cd-S distance of 2.7115(7) Å is common for the six coordinate thioether Cd(II) complexes.[14,55,87]

Crystal Structure of $Zn(L_2)_2(ClO_4)_2 \cdot H_2O$ (10). Similar to complex **9**, complex **10** contains a cation $[Zn(\mathbf{L_2})_2]^{2+}$ (Figure 12), two perchlorate anions and a non-coordinated water molecule. The intraligand S-M-N_{alkyl} and N-M-N bond angles are much larger than those in complex **8** and **9**. The intraligand S-M-$N_{pyridyl}$ bond angle is similar to that found in complex **9**. In contrast, the interligand S-M-N_{alkyl} and N_{alkyl}-M-$N_{pyridyl}$ bond angles are smaller than those in complex **8** and **9**. As expected, shorter M-N and M-S distances are observed in complex **10** due to the smaller ionic radius of zinc. The Zn-$N_{pyridyl}$ distance of 2.1059(19) Å is normal for six coordinate Zn(II) complex.[14,26,47-50] The Zn-N_{alkyl} distance of 2.1773(17) Å is on the short end of those (2.181-2.205 Å) found in the six-coordinate Zn(II) complex $[Zn(TATC)](ClO_4)_2$.[86] The Zn-S bond distance is 2.5978(13) Å, which is in the known range for the six-coordinate thioether-containing complexes.[55,88,89]

Table 15. Selected bond distances (Å) and bond angles (deg) for complex **11**

Bond Distances		Bond Angles	
Zn-N(2)	2.0936(16)	N(2)-Zn-N(1)	77.77(6)
Zn-N(1)	2.1346(16)	N(2)-Zn-Cl(1)	122.88(4)
Zn-Cl(1)	2.2449(5)	N(1)-Zn-Cl(1)	99.56(4)
Zn-Cl(2)	2.2504(5)	N(2)-Zn-Cl(2)	116.99(4)
Zn-S	2.8216(6)	N(1)-Zn-Cl(2)	99.41(5)
		Cl(1)-Zn-Cl(2)	119.641(19)
		N(2)-Zn-S	78.32(4)
		N(1)-Zn-S	156.03(4)
		Cl(1)-Zn-S	91.95(2)
		Cl(2)-Zn-S	92.90(2)

Symmetry transformations used to generate equivalent atoms: -x, -y + 2, -z+2

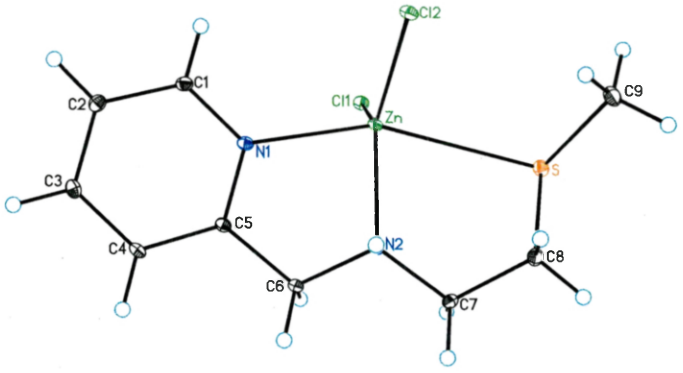

Figure 13. Structure of $Zn(\mathbf{L_2})Cl_2$ (**11**). Thermal ellipsoids are shown at the 50% level.

Crystal Structure of $Zn(\mathbf{L_2})Cl_2$ (11). As shown in Figure 13, complex **11** adopts a distorted trigonal bipyramidal geometry (τ = 0.55)[68] with the amine nitrogen and two chloride atoms defining the equatorial plane and the sulfur and pyridyl nitrogen at the axial positions. Similar geometry was observed in complex $Hg(\mathbf{L_2})Cl_2$.[36] The angles between the atoms in the equatorial plane are approximately ideal, ranging from 116.99(4)° to 122.88(4)°. However, the $N_{pyridyl}$-Zn-S bond angles of 156.03(4)° deviate significantly from linearity. The Zn-$N_{pyridyl}$ distance of 2.1346 (16) Å is comparable to

those found in complex **6** and other five coordinate Zn(II) complex.[26,90] The Zn-N_{alkyl} of 2.0936(16) Å is typical for the five-coordinate Zn(II) complex.[90] The Zn-S distance is 2.8216(6) Å, which is significantly larger than those found in complex **6** and $[Zn(\mathbf{L_1}^2)Br_2]$.[35]

Table 16. Selected bond distances (Å) and bond angles (deg) for complexes **12** and **13**

$Hg(L_3)_4(ClO_4)_4$·6 acetone (**12**)[a]		$Cd_3(\mathbf{L_3})_3(ClO_4)(CO_3)\cdot H_2O$ (**13**)[b]	
Hg(1)-N(1A)	2.480(3)	Cd-O	2.230(2)
Hg(1)-S(1B)#1	2.4841(9)	Cd-N(1)	2.357(4)
Hg(1)-S(1A)	2.4941(10)	Cd-S(1)#1	2.4888(19)
Hg(1)-N(2A)	2.513(3)	Cd-N(2)	2.536(3)
Hg(1)-S(2A)	2.7306(10)	Cd-S(1)	2.554(2)
Hg(2)-N(1B)	2.410(3)	Cd-O#2	2.690(3)
Hg(2)-S(1B)	2.5214(9)		
Hg(2)-S(1A)	2.5279(9)		
Hg(2)-N(2B)	2.559(3)		
Hg(2)-S(2B)	2.6063(11)		
N(1A)-Hg(1)-S(1B)#1	87.14(8)	O-Cd-N(1)	80.96(7)
N(1A)-Hg(1)-S(1A)	111.78(8)	O-Cd-S(1)#1	124.35(5)
S(1B)#1-Hg(1)-S(1A)	130.53(3)	N(1)-Cd-S(1)#1	101.11(5)
N(1A)-Hg(1)-N(2A)	68.21(10)	O-Cd-N(2)	116.61(7)
S(1B)#1-Hg(1)-N(2A)	146.77(7)	N(1)-Cd-N(2)	68.82(8)
S(1A)-Hg(1)-N(2A)	80.86(8)	S(1)#1-Cd-N(2)	115.59(5)
N(1A)-Hg(1)-S(2A)	121.64(8)	O-Cd-S(1)	97.14(5)
S(1B)#1-Hg(1)-S(2A)	99.44(3)	N(1)-Cd-S(1)	139.05(7)
S(1A)-Hg(1)-S(2A)	106.84(3)	S(1)#1-Cd-S(1)	112.83(5)
N(2A)-Hg(1)-S(2A)	76.98(7)	N(2)-Cd-S(1)	76.05(8)
N(1B)-Hg(2)-S(1B)	125.15(8)	O-Cd-O#2	52.35(8)
N(1B)-Hg(2)-S(1A)	95.06(8)	N(1)-Cd-O#2	81.51(6)
S(1B)-Hg(2)-S(1A)	103.38(3)	S(1)#1-Cd-O#2	72.73(4)
N(1B)-Hg(2)-N(2B)	70.18(11)	N(2)-Cd-O#2	150.11(7)
S(1B)-Hg(2)-N(2B)	79.68(8)	S(1)-Cd-O#2	129.24(4)
S(1A)-Hg(2)-N(2B)	162.91(8)		
N(1B)-Hg(2)-S(2B)	101.96(9)		
S(1B)-Hg(2)-S(2B)	115.90(3)		
S(1A)-Hg(2)-S(2B)	113.82(3)		
N(2B)-Hg(2)-S(2B)	78.70(8)		

[a]Symmetry transformations used to generate equivalent atoms: -x+1, y, -z+1/2

[b]Symmetry transformations used to generate equivalent atoms: y-1/3, -x+y+1/3, -z+4/3; -x+y, -x+1, z; -x+y-1, -x, z; -y, x-y+1, z; x-y+2/3, x+1/3, -z+4/3; -y+1, x-y+1, z

III. Crystal Structures of L_3-Containing Metal Complexes

In the solid-state $\mathbf{L_3}$ acts as a bridging ligand forming two thiolate-bridged polymeric structures in complex **12** and **13** as shown in Figures 14 and 15. The thiolate-bridging feature was previously reported for the related complexes $[Zn_4(L)_4]$ (LH_2 = N, N-bis(2-mercaptoethyl)benzylamine).[25] In complex **12**, $\mathbf{L_3}$ binds Hg(II) in a tetradentate fashion. In complex **13**, $\mathbf{L_3}$ is only tridentate and the thioether moiety is pendant to the metal center.

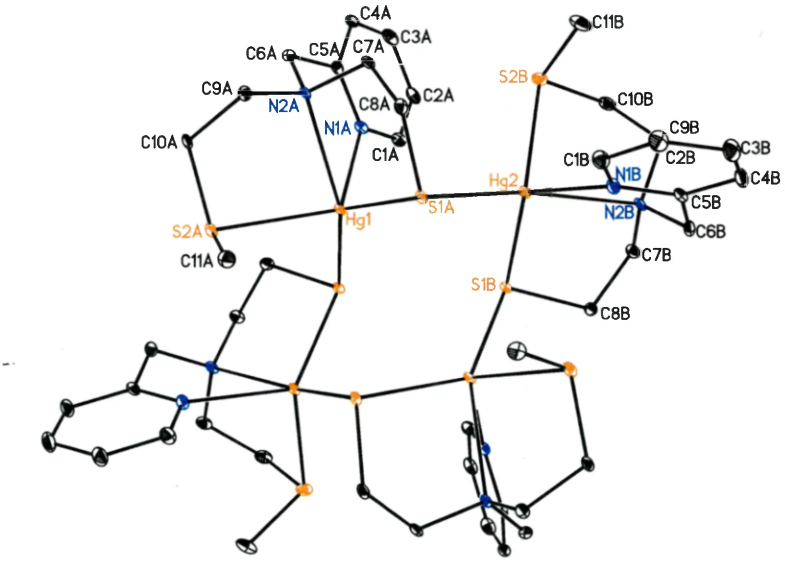

Figure 14. Structure of the cation of $[Hg_4(\mathbf{L_3})_4](ClO_4)_4 \cdot 6$acetone (**12**). Thermal ellipsoids are shown at the 50% level.

Crystal Structure of $[Hg_4(L_3)_4](ClO_4)_4 \cdot 6$acetone (12). In the solid-state complex **12** contains a tetramer, which consists of four Hg(II) centers linked by four independent thiolate moieties, and six non-coordinating acetone molecules. In complex **12**, two types of five-coordinate Hg(II) geometries are produced. Hg(1) has a distorted tetragonal geometry ($\tau = 0.42$)[68] with S(1A) occupying the apical position and N(1A), N(2A), S(2A)

and S(1B) at the basal positions. The angles between atoms in the basal plane are 68.21(10)°, 76.98(7)°, 87.14(8)° and 99.43(3)° for N(1A)-Hg(1)-N(2A), N(2A)-Hg(1)-S(2A), N(1A)-Hg(1)-S(1B) and S(1B)-Hg(1)-S(2A), respectively. Hg(2) has a distorted trigonal bypyramidal (τ = 0.63)[68] geometry. The axial positions are occupied by S(1A) and N(2B) with a S(1A)-Hg(2)-N(2B) bond angle of 162.91(8)°. Hg(2) is located ~1.0 Å from the equatorial plane defined by S(1B), S(2B) and N(1B). The Hg-$N_{pyridyl}$ distances of 2.480(3) and 2.410(3) Å are comparable to those in complex **4** and Hg(**L_2**)Cl_2.[36] The Hg-N_{alkyl} distances of 2.513(3) and 2.559(3) Å are in the observed range for the five-coordinate Hg(II) complexes.[7,8,70,91] The Hg-$S_{thiolate}$ bond lengths of 2.5279(9) and 2.4941(10) Å are shorter than the Hg-$S_{thioether}$ bond lengths of 2.6063(11) and 2.7306(10) Å, consistent with the increased donor capacity of thiolate sulfurs in comparison with thioether sulfurs.

Crystal Structure of [$Cd_3(L_3)_3(CO_3)$](ClO_4)·0.5H_2O (13). As shown in Figure 15, complex **13** has a hexameric structure with the six Cd(II) linked by two carbonate and six independent thiolate moieties. The carbonate was apparently derived from carbon dioxide in air. The six-coordinate Cd(II) has a highly distorted octahedral geometry with the pyridyl N and thiolate S from the same ligand occupying the axial positions, and two carbonate oxygens, the alkylamino N and the bridging thiolate S (from another ligand) in the equatorial plane. Unlike complex **12**, the thioether moiety is located far away from the coordination sphere, resulting a tridentate ligand binding mode. The Cd-$N_{pyridyl}$ distance of 2.357(4) Å is comparable to those found in complexes **2** and **9**, but the Cd-N_{alkyl} distance of 2.536(3) Å is obviously longer than that in complex **9**. Cd-$S_{thiolate}$

distance of 2.554(2) Å is longer that those in complex **12,** indicating weaker bonding between Cd(II) and the thiolate sulfur.

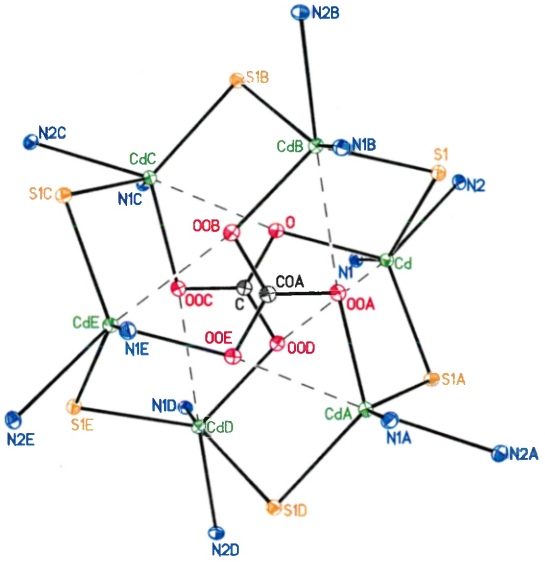

Figure 15. Structure of the cation of $[Cd_3(\mathbf{L_3})_3(CO_3)](ClO_4)\cdot 0.5H_2O$ **(13)**. Thermal ellipsoids are shown at the 50% level;

IV. Solution-State ^{1}H NMR Spectroscopy

Investigation of L_1[1] coordination of divalent zinc triad metals in the solution state. Metal ion binding to $\mathbf{L_1}$[1] with the perchlorate and chloride salts of divalent zinc triad metals were studied in the solution state using ^{1}H NMR spectroscopy. The room temperature acetonitrile-d_3 solution ^{1}H chemical shifts for complexes **1-3** are generally downfield of equivalent resonances for the free ligand. Downfield shifts are generally observed upon complexation to metal ions and attributed to the deshielding influence of σ donation to the metal center. Complexes **1-3** and **4-6** exhibited similar ^{1}H chemical shifts, respectively, with no apparent periodic trends. The labeling scheme for the protons is shown in Figure 1.

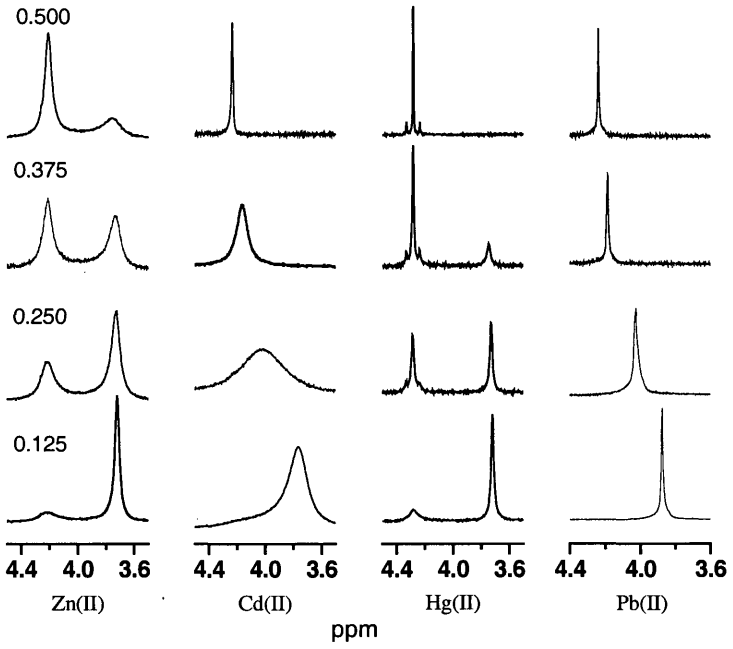

Figure 16. Methylene (H_f) region of the ^1H NMR spectra for $\mathbf{L_1}^1$ at −40 °C in acetonitrile-d_3 as a function of added $M(ClO_4)_2$ with nominal $[M^{2+}]/[\mathbf{L_1}^1] = 0.125$, 0.250, 0.375 and 0.500. Nominal total $[M^{2+}] = 2$ mM.

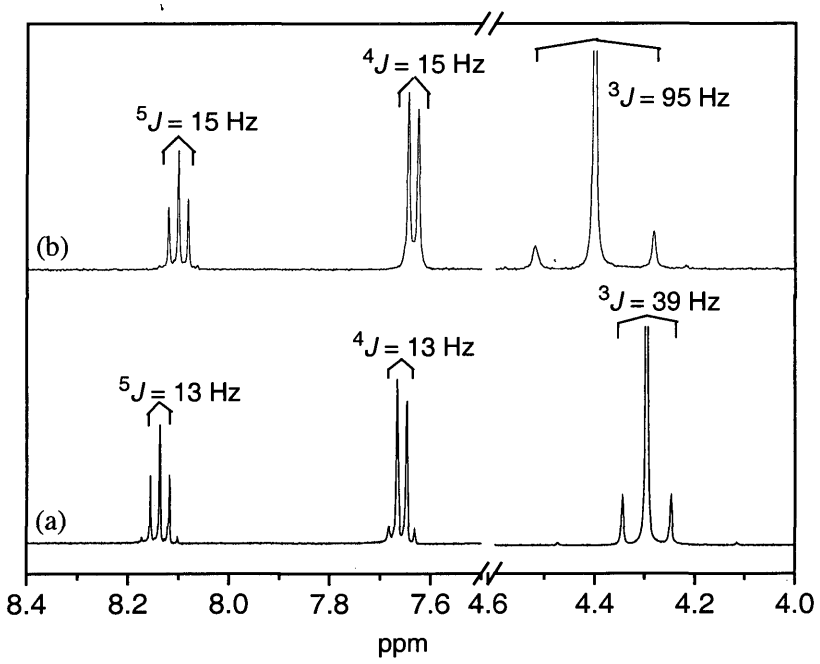

Figure 17. Selected ^1H NMR spectra in CD_3CN with total [Hg(II)] = 2 mM at −20 °C (a) $[Hg(\mathbf{L_1}^1)_2]^{2+}$; (b) $[Hg(\mathbf{L_1}^1)]^{2+}$.

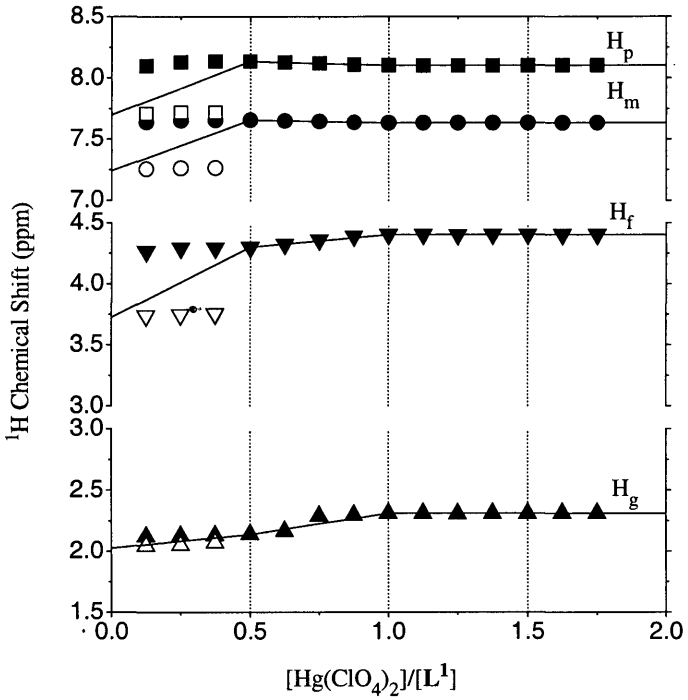

Figure 18. Chemical shifts of the protons of $\mathbf{L_1}^1$ in the presence of $Hg(ClO_4)_2$ as a function of the nominal metal-to-ligand ratios in CD_3CN at –20 °C. Open symbols represent the chemical shifts of the free ligands, and closed symbols represent the chemical shifts of the complexed ligands. Lines represent the chemical shift expected for rapid exchange between $M(\mathbf{L_1}^1)_2^{2+}$ and free ligand for $[M(ClO_4)_2]/[\mathbf{L_1}^1] < 0.5$, rapid exchange between $M(\mathbf{L_1}^1)_2^{2+}$ and $M(\mathbf{L_1}^1)^{2+}$ for $0.5 < [M(ClO_4)_2]/[\mathbf{L_1}^1] < 1.0$, and slow exchange between $M(\mathbf{L_1}^1)^{2+}$ and M^{2+} for $[M(ClO_4)_2]/[\mathbf{L_1}^1] > 1.0$.

The coordination chemistry of $\mathbf{L_1}^1$ binding to divalent group 12 metal perchlorates in acetonitrile-d_3 solutions was investigated by ^{1}H NMR at room temperature, –20 °C and –40 °C with nominal $[M(ClO_4)_2]/[\mathbf{L_1}^1]$ molar ratios between 0.125 and 1.75 and total $[M(ClO_4)_2]$ = 2 mM. Spectral trends indicated that formation of $M(\mathbf{L_1}^1)_2^{2+}$ was favored thermodynamically over formation of $M(\mathbf{L_1}^1)(NCCH_3)_x^{2+}$ for $[M(ClO_4)_2]/[\mathbf{L_1}^1] < 0.5$ with all three metal ions (Figures 16, 18, 19 and 20). At –40 °C, sharp peaks for the free ligand gradually lost intensity as $[Hg(ClO_4)_2]/[\mathbf{L_1}^1]$ was increased to 0.5 and a new set of

sharp peaks increased in intensity. Spectral trends indicated $[Hg(\mathbf{L_1}^1)_2]^{2+}$ and free ligand were in slow exchange on the chemical shift time scale and coupling constant time scale at low $[Hg(ClO_4)_2]/[\mathbf{L_1}^1]$. In contrast, a single set of shifting broadened ligand resonances was observed as a function of $[Cd(ClO_4)_2]/[\mathbf{L_1}^1]$ under similar conditions indicating behavior approaching rapid exchange on the chemical shift time scale. Interestingly, two sets of slightly broadened ligand resonances with invariable chemical shifts were observed as a function of $[Zn(ClO_4)_2]/[\mathbf{L_1}^1]$ under similar conditions revealing behavior approaching slow exchange on the chemical shift time scale. Previous investigation of zinc triad binding to the NSN donor ligand bis(2-methylpyridyl) sulfide also provided some examples of Zn^{2+} coordination behavior being more similar to Hg^{2+} coordination behavior than Cd^{2+}.[14]

Complexes **1** and **2** were also examined for evidence of slow exchange on the $J(M^1H)$ time scale. For complex **1**, $^{3\text{-}5}J(^{199}Hg^1H)$ were observed in acetonitrile-d_3 at –40 °C (Figure 17a, Table 17), and an invariant NMR spectrum was obtained over a week at room temperature indicating **1** was stable in acetonitrile-d_3 solution. The large magnitude of $J(^{199}Hg^1H)$ to H_g indicates that the thioether sulfur are bound to the metal center. Since neither $J(^{199}Hg^1H)$ for a bidentate nitrogen and/or sulfur ligand nor $^6J(^{199}Hg^1H)$ for a coordination compound have ever been reported, the pyridyl nitrogens are probably bound to Hg^{2+} in solution as observed in the crystal structure of **1**. However, there are nine isomeric forms of bis-tridentate chelates.[12] The NMR spectrum observed has a single environment for all ligand protons and is consistent with either the meridional structure observed in the solid state or rapid exchange between all nine isomeric forms. Interconversion of the isomeric forms requires rotation about pseudo-C_3 axes of the

trigonal prismatic and pseudo-octahedral cores of ligating atoms. The energy differences between different isomeric forms are particularly small when all M-L bond distances are equal. In **1**, the Hg-N bond lengths are shorter than the M-S bond lengths by 0.27 and 0.35 Å. These differences are somewhat greater than the 0.2 Å range between Hg-N of $Hg(BMPA)^{2+}$ which was determined to exist as an equilibrium mixture of all but the meridional isomer. While an invariant NMR spectrum was also obtained for complex **2**, conditions for detection of $J(^{111/113}Cd^{1}H)$ could not be found in acetonitrile-d_3 solution, even under conditions with excess metal ion.

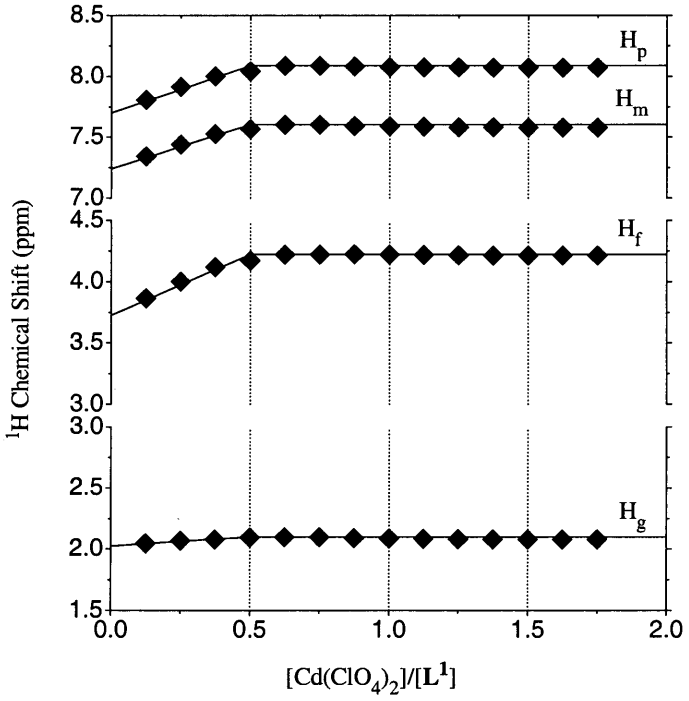

Figure 19. Chemical shifts of the protons of $\mathbf{L_1}^1$ in the presence of $Cd(ClO_4)_2$ as a function of the nominal metal-to-ligand ratios in CD_3CN at −20 °C. Lines represent the expected chemical shifts as described in Figure 18.

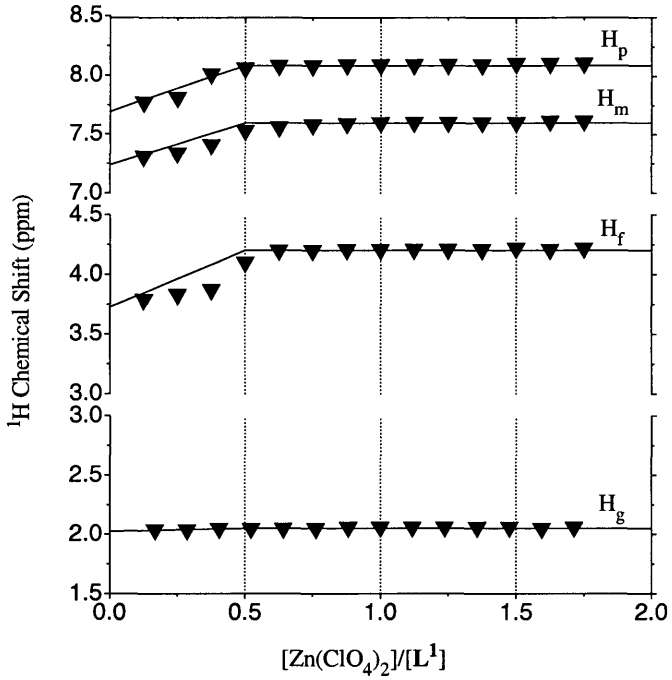

Figure 20. Chemical shifts of the protons of $\mathbf{L_1}^1$ in the presence of $Zn(ClO_4)_2$ as a function of the nominal metal-to-ligand ratios in CD_3CN at −20 °C. Lines represent the expected chemical shifts as described in Figure 18.

Examination of the divalent zinc triad perchlorate coordination behavior of $\mathbf{L_1}^1$ at $[M(ClO_4)_2]/[\mathbf{L_1}^1]$ molar ratios greater than 0.5 also revealed differences in behavior. With Hg^{2+}, downfield shifts of 0.10 and 0.17 ppm for H_f and H_g, respectively, and upfield shifts of 0.02 and 0.03 ppm for H_m and H_p, respectively, occurred in a linear fashion between $[Hg(ClO_4)_2]/[\mathbf{L_1}^1]$ molar ratios of 0.5 and 1.0 (Figure 22). The chemical shift changes were smaller in magnitude than the difference in chemical shift between the free ligand and $Hg(\mathbf{L_1}^1)_2^{2+}$. In addition, the magnitudes of $J(^{199}Hg^1H)$ to all the ligand protons increased (Figure 17, Table 17). The changes in the ^1H NMR of the ligand for $[Hg(ClO_4)_2]/[\mathbf{L_1}^1]$ between 0.5 and 1 indicated that $Hg(\mathbf{L_1}^1)(NCCH_3)_x^{2+}$ was thermodynamically more stable than $[Hg(\mathbf{L_1}^1)_2]^{2+}$ under these conditions. The ligand

proton chemical shifts remained constant at $[Hg(ClO_4)_2]/[\ \mathbf{L_1}^1] > 1$ but the ^{199}Hg coupling satellites (Figure 17b) became exchange broadened indicating ligand exchange between solvated Hg^{2+} and $Hg(\mathbf{L_1}^1)(NCCH_3)_x^{2+}$. In contrast, the proton NMR spectra of $Cd(\mathbf{L_1}^1)_2^{2+}$, $Zn(\mathbf{L_1}^1)_2^{2+}$ remained essentially invariant in solutions with $[M(ClO_4)_2]/[\ \mathbf{L_1}^1] > 0.625$. This suggests that $M(\mathbf{L_1}^1)_2^{2+}$ is more thermodynamically stable than $M(\mathbf{L_1}^1)(NCCH_3)_x^{2+}$ for $M = Cd^{2+}$ and Zn^{2+} over the range of $[M(ClO_4)_2]/[\ \mathbf{L_1}^1]$ examined (Figure 22). However, the changes in $J(^{199}Hg^1H)$ were more definitive than the changes in proton chemical shift for the interconversion of $Hg(\mathbf{L_1}^1)_2^{2+}$ and $Hg(\mathbf{L_1}^1)(NCCH_3)_x^{2+}$. Since $J(^{111/113}Cd^1H)$ was never detected for the Cd^{2+} complexes and zinc does not have a favorable isotope for NMR detection, the $M{:}\mathbf{L_1}^1$ stoichiometry of the Cd^{2+}, Zn^{2+} and complexes at $[M(ClO_4)_2]/[\ \mathbf{L_1}^1] > 0.5$ is ill-defined in solution.

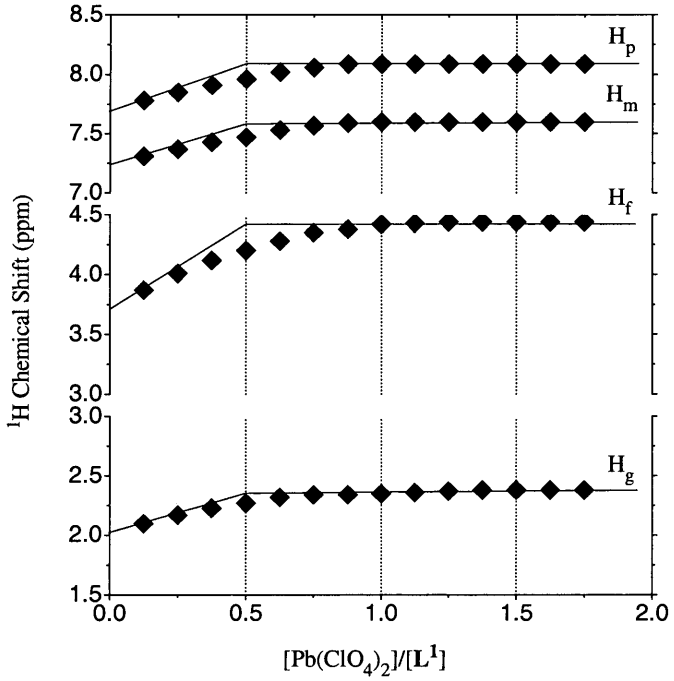

Figure 21. Chemical shifts of the protons of $\mathbf{L_1}^1$ in the presence of $Pb(ClO_4)_2$ as a function of the nominal metal-to-ligand ratios in CD_3CN at −20 °C. Lines represent the expected chemical shifts as described in Figure 18.

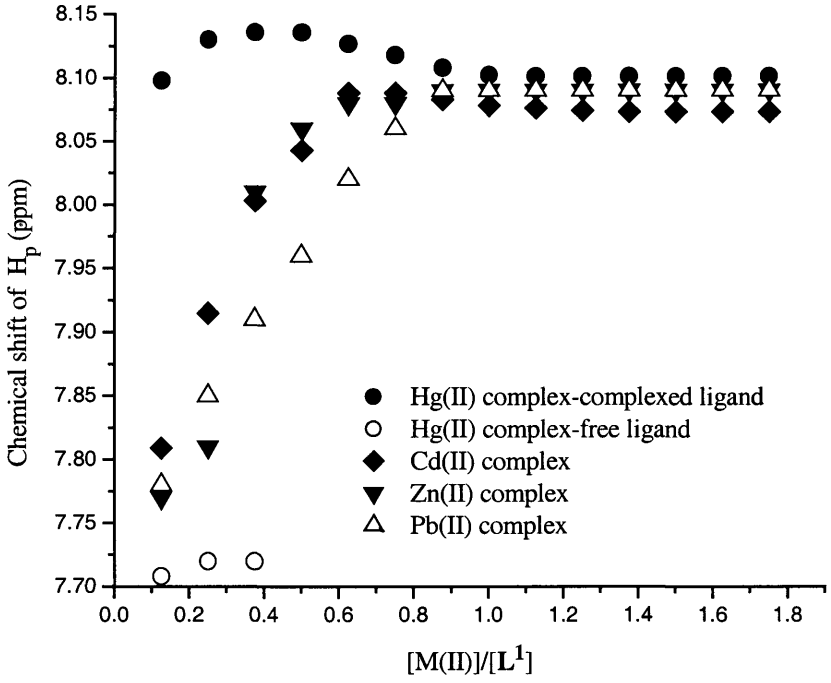

Figure 22. Comparison of the chemical shift trends for H_p as a function of [M(II)]/($\mathbf{L_1}^1$) in acetonitrile-d_3 at −20 °C with nominal total [M(II)] = 2 mM.

Comparable solution equilibria have been reported for the Hg(II) coordination chemistry of related tridentate ligands.[12,14] The observed $^3J(^{199}Hg^1H)$ for $Hg(\mathbf{L_1}^1)(NCCH_3)_x^{2+}$ of 105 and 95 Hz $^3J(^{199}Hg^1H)$ are among the largest couplings constants reported for thioether ligand-containing Hg(II) complexes.[14,92] Reports of longer range $J(^{199}Hg^1H)$ in Hg(II) coordination compounds are rare. Those reported here fall in the known range of 8 to 30 Hz for coupling between ^{199}Hg and ^1H seperated by four or five bonds.[7,9,12,14,16,93]

The coordination chemistry of $\mathbf{L_1}^1$ binding to divalent group 12 metal chlorides in acetonitrile-d_3 solutions was also investigated by ^1H NMR. Crystals of **5** were sparingly soluble in acetronitrile-d_3. However, no $J(M^1H)$ couplings were found for complexes **5**

and **6** at –20 °C and –40 °C with $[M^{2+}]$ = 2 mM, in acetonitrile-d_3. Previous work suggests that ligand exchange of d^{10} metal ions with coordinating counter ions such as chloride ions occurs particularly rapidly because of reductions in the available charge density. Precedent for detection of HgH couplings in coordination compounds of $HgCl_2$ is limited to tetradentate chelating ligands.[7,13,70]

Table 17. $J(^{199}Hg^{1}H)$ constants for 1:1 and 1:2 Hg(II) complexes of $\mathbf{L_1}^1$ with Hg(II) = 2 mM in acetonitrile-d_3 at –40 °C.

Proton	$Hg(\mathbf{L_1}^1)_2^{2+}$	$Hg(\mathbf{L_1}^1)(CH_3CN)_x^{2+}$
H_p	13	15
H_m	13	15
H_f	39	95
H_g	49	105

Investigation of $\mathbf{L_1}^1$ coordination of Pb(II) in the solution state. The solution-state coordination chemistry of $\mathbf{L_1}^1$ binding to $Pb(ClO_4)_2$ in acetonitrile-d_3 solutions was also investigated by ^1H NMR under the similar conditions used for studying the zinc triad complexes. For comparison with the zinc triad metal complexes, the chemical shifts of the ligand resonances are plotted as a function of $[Pb(ClO_4)_2]/[\mathbf{L_1}^1]$ in Figure 21. At –40 °C, a single set of sharp, shifting ligand resonances was observed in the range of $0 < [Pb(ClO_4)_2]/[\mathbf{L_1}^1] < 0.5$, revealing the rapid exchange on the chemical shift time scale (Figure 16). Further down field shifting was observed for the ligand resonances when the molar ratio of Pb(II) was increased to 0.875. Invariant spectra were obtained at the $[Pb(ClO_4)_2]/[\mathbf{L_1}^1]$ molar ratios greater than 0.875. Slow exchange conditions for detection of $J(^{207}Pb^{1}H)$ were never found for $Pb(ClO_4)_2/\mathbf{L_1}^1$ in acetonitrile-d_3 solution even under conditions with excess metal ion. The weaker bonding of Pb(II) to the sulfur donors and coordination of the perchlorate counter ions may contribute to absence of $J(^{207}Pb^{1}H)$ in

solutions containing $\mathbf{L_1}$[1] and Pb(II). Further studies are required to establish conditions favoring slow exchange behavior for Pb(II) complexes of small biologically relavent ligands.

Investigation of L_2 coordination of divalent zinc triad metals in the solution state. Metal ions binding to $\mathbf{L_2}$ with the perchlorate salts of divalent zinc triad metals were studied in the solution state using ^{1}H NMR spectroscopy. The ^{1}H NMR of $\mathbf{L_2}$ consists of four resonances in the aromatic region associated with protons H_a through H_d, a singlet corresponding to the methylene (H_f and H_f'), two triplets corresponding to the ethylene protons (H_g, Hg', H_h and H_h'), and a singlet resonance corresponding to the methyl protons H_i. The labeling scheme for the protons of $\mathbf{L_2}$ is shown in Figure 2.

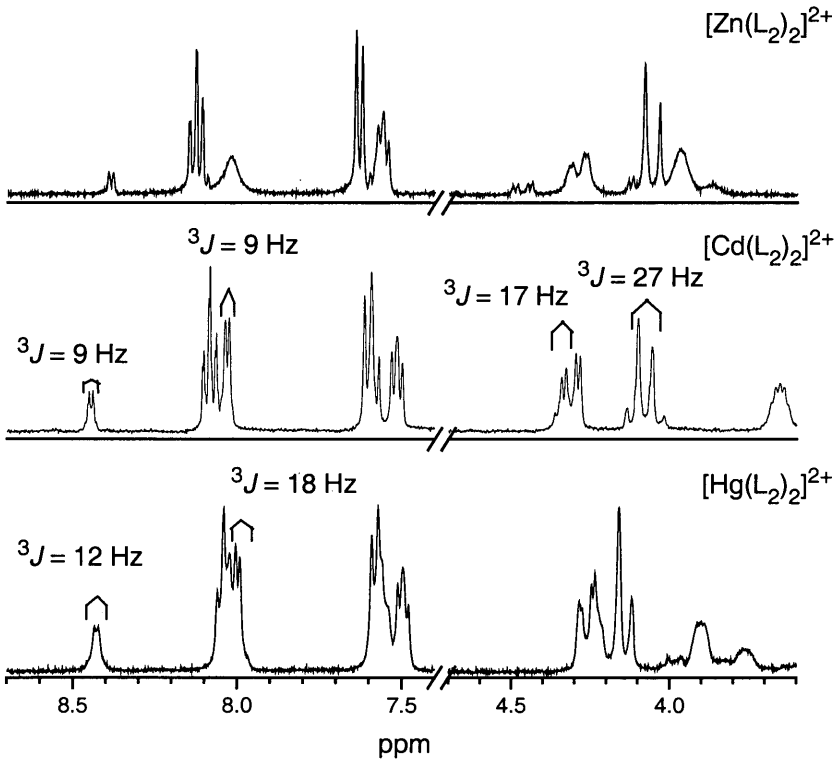

Figure 23. Highlightes of the ^{1}H NMR spectra of $[M(\mathbf{L_2})_2]^{2+}$ in CD_3CN with total [M(II)] = 2 mM at −40 °C.

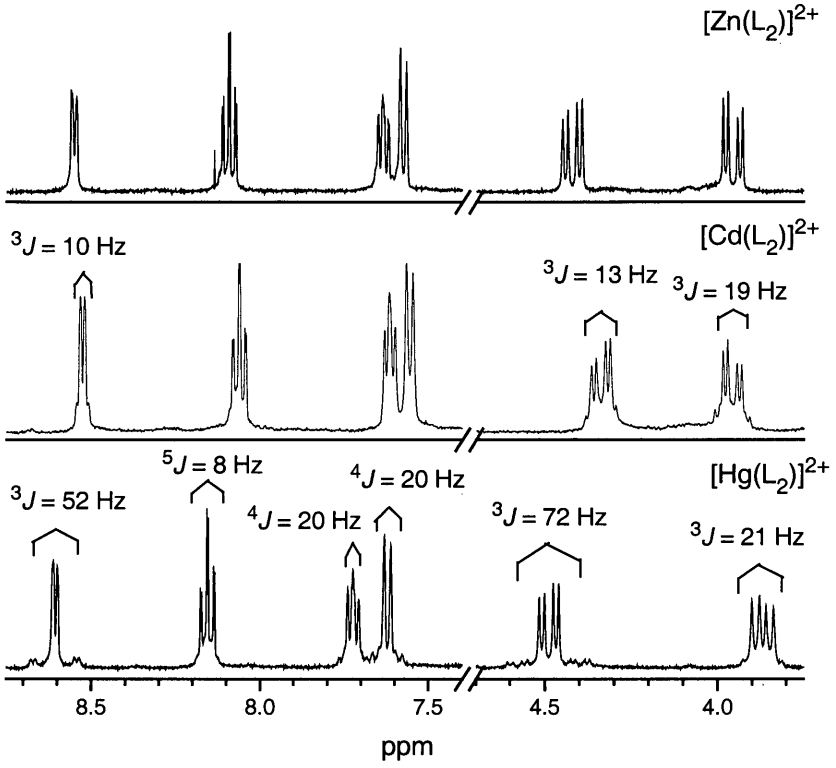

Figure 24. Highlightes of the ^{1}H NMR spectra of $[M(\mathbf{L_2})(CD_3CN)_x]^{2+}$ in CD_3CN with total [M(II)] = 2 mM at 20 °C.

The coordination chemistry of $\mathbf{L_2}$ binding to divalent group 12 metal perchlorates in acetonitrile-d_3 solutions was investigated by ^{1}H NMR spectroscopy at room temperature and –40 °C with nominal $[M(ClO_4)_2]/[\mathbf{L_2}]$ molar ratios between 0.125 and 1.625 with total $[M(ClO_4)_2]$ = 2 mM. Since the ethylene group was diastereoctopic and broadened upon metal ion coordination, and the methyl group was in close proximity to the solvent and water peaks, the pyridine and methylene hydrogens were the focus of solution-state coordination chemistry studies. Spectral trends revealed the existence of 1:2 and 1:1 metal-to-$\mathbf{L_2}$ complexes for the zinc triad in solution. As shown in Figure 23, at –40 °C slow exchange conditions were observed for $Hg(\mathbf{L_2})_2^{2+}$ and $Cd(\mathbf{L_2})_2^{2+}$ on the

chemical shift and coupling constant time scales and for $Zn(\mathbf{L_2})_2^{2+}$ on the chemical shift time scale. Three-bond heteronuclear couplings $^3J(M^1H)$ were observed for the $Hg(\mathbf{L_2})_2^{2+}$ and $Cd(\mathbf{L_2})_2^{2+}$ cations. Similar proton resonances were observed for all three $M(\mathbf{L_2})_2^{2+}$ cations, and followed the trends $\delta(Hg(\mathbf{L_2})_2^{2+}) < \delta(Cd(\mathbf{L_2})_2^{2+}) < \delta(Zn(\mathbf{L_2})_2^{2+})$ for the pyridine protons, but $\delta(Hg(\mathbf{L_2})_2^{2+}) > \delta(Cd(\mathbf{L_2})_2^{2+}) > \delta(Zn(\mathbf{L_2})_2^{2+})$ for the methylene protons. Two environments for H_a with different mole fractions were found in the solution state at –40 °C. Significantly, both of these H_a environments exhibited metal coupling satellites in the presence of either ^{199}Hg or $^{111/113}Cd$. Slow exchange on the chemical shift and coupling constant time scales between two isomeric forms of bis-tridentate chelates may be responsible for this observation.[12] The relatively small changes in the chemical shifts of other protons with the addition of metal possibly contribute to the inability to detect dual environments for the other ligand protons. The methylene protons exhibited a diastereotopic splitting pattern suggesting the amine nitrogen was coordinated to the metal ions in $M(\mathbf{L_2})_2^{2+}$ cations.

Slow exchange conditions on the chemical shift time scale were also found for 1:1 metal-to-ligand complexes of $\mathbf{L_2}$ with the entire zinc triad, and on the coupling constant time scale with Hg(II) and Cd(II). Similar proton resonances were found in all three cations $M(\mathbf{L_2})(NCCH_3)_x^{2+}$ with the trend $\delta(Hg(\mathbf{L_2})^{2+}) > \delta(Cd(\mathbf{L_2})^{2+}) \approx \delta(Zn(\mathbf{L_2})^{2+})$. Moreover, except for small temperature effects on the proton chemical shifts ($\leq$ 0.05 ppm), the spectra from 3.5 to 9 ppm were identical to those taken at room temperature (Figure 24). For the $Hg(\mathbf{L_2})(NCCH_3)_x^{2+}$ cation, heteronuclear couplings $^{3\text{-}5}J(^{199}Hg^1H)$ were observed for all pyridyl, methylene and methyl protons. In the comparable Cd(II) complex, heteronuclear couplings between ^{113}Cd and protons four or more bonds away

were not observed. Only the pyridyl proton H_a, which has the closest proximity to the pyridyl nitrogen, was coupled Cd(II). The methylene and methyl protons were also both coupled to Cd(II).

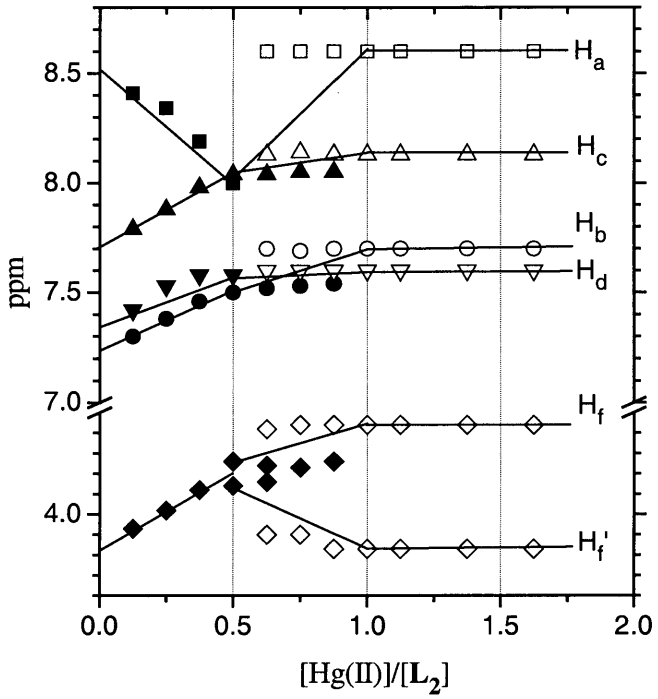

Figure 25. Chemical shifts of the protons of $\mathbf{L_2}$ in the presence of $Hg(ClO_4)_2$ as a function of the nominal metal-to-ligand ratios in CD_3CN at –40 °C. Lines represent the chemical shift expected for rapid exchange between $M(\mathbf{L_2})_2^{2+}$ and free ligand for $[M(ClO_4)_2]/[\mathbf{L_2}] < 0.5$, rapid exchange between $M(\mathbf{L_2})_2^{2+}$ and $M(L_2)^{2+}$ for $0.5 < [M(ClO_4)_2]/[\mathbf{L_2}] < 1.0$, and slow exchange between $M(\mathbf{L_2})^{2+}$ and M^{2+} for $[M(ClO_4)_2]/[\mathbf{L_2}] > 1.0$.

At $[M(ClO_4)_2]/[\mathbf{L_2}] < 0.5$, the formation of $M(\mathbf{L_2})_2^{2+}$ was favored thermodynamically over formation of $M(\mathbf{L_2})(NCCH_3)_x^{2+}$ for the zinc triad. At –40 °C, a single set of shifting broadened pyridine hydrogen resonances was found as a function of $[Cd(ClO_4)_2]/[\mathbf{L_2}]$ and $[Hg(ClO_4)_2]/[\mathbf{L_2}]$, which changed approximately linearly with $[M(II)]/[\mathbf{L_2}]$ as predicted for the rapid exchange between free ligand and the 1:2 metal-to-

ligand complex (Figures 25 and 26). In contrast, two sets of broadened pyridyl hydrogen resonances with approximately invariable chemical shifts were observed as a function of $[Zn(ClO_4)_2]/[\mathbf{L_2}]$ (Figure 27), providing evidence for slow exchange on the chemical shift time scale. Broadened peaks for the free ligand gradually lost intensity as $[Zn(ClO_4)_2]/[\mathbf{L_2}]$ was increased to 0.5 and a new set of sharp peaks increased in intensity. This result revealed that Hg(II) and Cd(II) exhibit similar coordination behavior in the solution state upon the coordination of $\mathbf{L_2}$ at low metal-to-ligand ratios, which was different from those observed in $\mathbf{L_1}$[1] metal complexes. This result also suggests that the rate of ligand exchange is dependent on the nature of the donor sets. It is also interesting to note that except for the hydrogen, which has the closest proximity to the pyridine nitrogen, all other selected ligand resonance shifted downfield for all three metals. Similar results were observed for Hg(II) and Cd(II) binding to BMPA (bis[2-pyridyl]methyl)amine).[10,12]

Examination of the divalent zinc triad perchlorate coordination behavior of $\mathbf{L_2}$ at $0.5 < [M(ClO_4)_2]/[\mathbf{L_2}] < 1.0$ revealed slow exchange conditions between $M(\mathbf{L_2})_2^{2+}$ and $M(\mathbf{L_2})(NCCH_3)_x^{2+}$ for all three metal ions as shown in Figures 25-27. The chemical shifts for one set of ^1H resonances, which were very close to those of $[M(\mathbf{L_2})_2]^{2+}$ cations, decreased in intensity as the equivalents of [M(II)] were increased, while the other set of ^1H resonances increased in intensity as the equivalents of [M(II)] were increased. No heteronuclear couplings $J(M^1H)$ were observed until $[M(II)]/[\mathbf{L_2}]$ reached 1.0 for Hg(II) and Cd(II). All of the protons at selected region shifted down field compared to the free ligands. Note that the chemical shift of the pyridyl proton H_a was most changed upon the

metal coordination, which can be explained by its closest proximity to the coordinating pyridyl nitrogen.

Further examination of the divalent zinc triad perchlorate coordination behavior of $\mathbf{L_2}$ at $[M(ClO_4)_2]/[\mathbf{L_2}] > 1.0$ revealed slow exchange conditions between M^{2+} and $[M(\mathbf{L_2})(NCCH_3)_x]^{2+}$ on the chemical shift and coupling constant time scales for Hg(II) and Cd(II), and on chemical shift time scale for Zn(II). Sharp peaks with constant chemical shifts for four pyridyl proton environments and two methylene proton environments were observed with 1.0–1.625 equivalent of M(II). Heteronuclear coupling between Hg(II) or Cd(II) and ligand protons retained within the region of 1.0–1.625 confirming the slow exchange conditions between solvated M^{2+} and $M(\mathbf{L_2})(NCCH_3)_x^{2+}$.

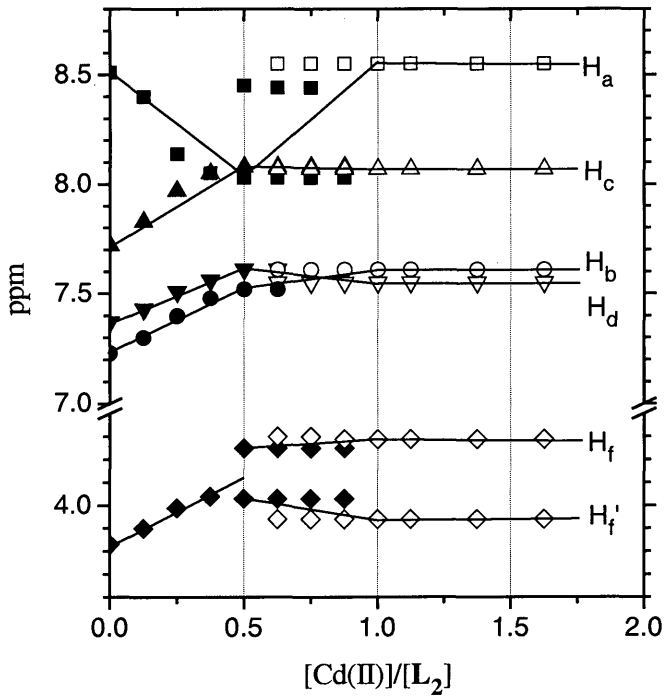

Figure 26. Chemical shifts of the protons of $\mathbf{L_2}$ in the presence of $Cd(ClO_4)_2$ as a function of the nominal metal-to-ligand ratios in CD_3CN at –40 °C. Lines represent the expected chemical shifts as described in Figure 24.

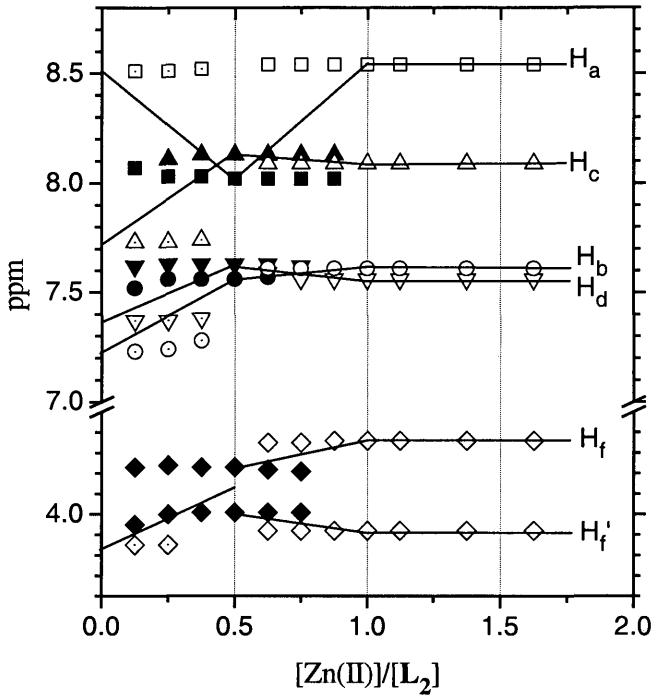

Figure 27. Chemical shifts of the protons of $\mathbf{L_2}$ in the presence of $Zn(ClO_4)_2$ as a function of the nominal metal-to-ligand ratios in CD_3CN at −40 °C. Lines represent the expected chemical shifts as described in Figure 24.

Comparable solution equilibria have been reported for the Hg(II) and Cd(II) coordination chemistry of related tridentate ligand BMPA.[10,12] The observed $^3J(^{199}Hg^1H)$ for $[Hg(\mathbf{L_2})_2]^{2+}$ of 12 and 18 Hz are in the range reported for thioether ligand-containing Hg(II) complexes.[14,92] The couplings of ^{199}Hg to methyl protons were evident but can not be measured due to its close proximity to the water and solvent peaks for cation $[Hg(\mathbf{L_2})_2]^{2+}$. For cation $[Hg(\mathbf{L_2})(NCCH_3)_x]^{2+}$, the observed $^3J(^{199}Hg^1H)$ falls in the long range of 21 to 113 Hz, which are larger that those for cation $[Hg(\mathbf{L_2})_2]^{2+}$, and the 113 Hz $J(^{199}Hg^1H)$ to methyl protons appears to be the greatest value observed over three bonds in the Hg(II) complexes with the thioether ligands. The 20 and 8 Hz $J(^{199}Hg^1H)$ to the

pyridine proton over four and five-bond are falling in the known range.[7,9,12,14,16,93] In both cations $[Cd(\mathbf{L_2})_2]^{2+}$ and $[Cd(\mathbf{L_2})(CD_3CN)_x]^{2+}$, only three-bond heteronuclear couplings $^3J(^{113}Cd^1H)$ were observed. The $^3J(^{113}Cd^1H)$ values of 9 to 27 Hz are comparable to the reported values.[19] As expected, Cd(II) coupling is much weaker than the related Hg(II) coupling.[10]

Table 18. $J(M^1H)$ constants for 1:1 and 1:2 Hg(II) and Cd(II) complexes of $\mathbf{L_2}$ with M(II) = 2 mM in acetonitrile-d_3 at –40 °C.

Complex	Proton	M = Hg(II)	M = Cd(II)
$[M(\mathbf{L_2})_2]^{2+}$	H_a	18	9
	H_a'	12	9
	H_f		17
	H_f'		27
$[M(\mathbf{L_2})(CD_3CN)_x]^{2+}$	H_a	52	10
	H_b	20	
	H_c	8	
	H_d	20	
	H_f	72	13
	H_f'	21	19
	H_i	113	14

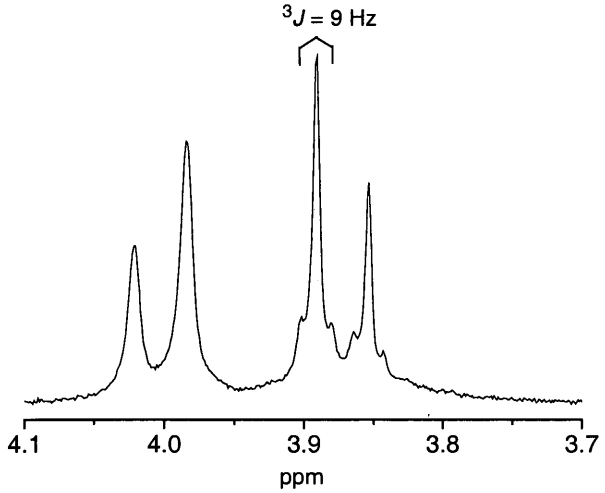

Figure 28. Highlights of the ^1H NMR spectrum of complex **13** in CD_3CN with total [M(II)] = 2 mM at 20 °C.

Extensive NMR studies of metal complexes of $\mathbf{L_3}$ in solution-state were precluded by its facile dimerization. However, the ^{1}H NMR spectrum of complex **13** at room temperature showed three bond heteronuclear coupling $^3J(^{113}Cd^1H)$ of 9 Hz to the methylene proton (Figure 28). No heteronuclear couplings were observed for complex **12** at either –40 °C or room temperature.

CONCLUSIONS

Tridentate binding modes for $\mathbf{L_1}^1$ and $\mathbf{L_2}$ were found in six divalent group 12 metal complexes in the solid-state. The binding of two ligands to the same metal center was first observed for pyridine-based dithioether ligands of type $\mathbf{L_1}$ in complexes $M(\mathbf{L_1}^1)_2(ClO_4)_2$ (M = Hg, Cd, Zn, Pb). Although $\mathbf{L_2}$ has not previously been used to investigate transition and heavy metal coordination chemistry, several Zn(II) complexes of the related thiolate ligand N-(2-mercaptoethyl)picolyamine (MEPAH) of Zn(II) complexes have been reported.[26] Also similar to MEPAH, $\mathbf{L_3}$ showed a great tendency to form thiolate-bridged polymers. The 1:2 metal-to-ligand complexes of $\mathbf{L_1}^1$ and $\mathbf{L_2}$ (**1-3** and **8-10,** respectively) all display distorted octahedral structures in the solid state with the two ligands in similar conformations. The formation of the five-membered chelating ring seems to be an important factor in deciding the molecular nature of these complexes. Complexes $Zn(\mathbf{L_1}^1)Cl_2$ and $Zn(\mathbf{L_2})Cl_2$ exist in the solid state as a monomer with distorted trigonal bipyramidal geometry. In contrast, monomeric complex $Hg(\mathbf{L_1}^1)Cl_2$ has a distorted square pyramidal geometry in the solid state. Complex $Cd_2(\mathbf{L_1}^1)_2Cl_4$ exists in the solid state as a dimer with the Cd(II) center in distorted octahedral coordination geometry. The tendency of $CdCl_2$ complexes to forming dimmers has previously been observed in $Cd_2(Py_2S)_2Cl_4$[14] and $Cd_2(L)_2Cl_4$ (L = 1-(5,6-dimethylbenz-imidazolyl)-3-benzimidazolyl-2-oxapropane).[73] Complexes $[Hg_4(\mathbf{L_3})_4](ClO_4)_4\cdot 6acetone$ (**12**) and $[Cd_3(\mathbf{L_3})_3(CO_3)](ClO_4)\cdot 0.5H_2O$ (**13**) exist in the solid state as thiolate-bridged polymers.

The observation of heteronuclear coupling between metal ions and ligand protons in ^1H NMR spectra facilitates investigation of the solution-state coordinating chemistry of ^{199}Hg and $^{111/113}Cd$ complexes. Slow exchange conditions permitting detection of small

long range $J(M^1H)$ were detected in 1:1 and 1:2 $Hg(ClO_4)_2$:$\mathbf{L_1^1}$, $Hg(ClO_4)_2$:$\mathbf{L_2}$ and $Cd(ClO_4)_2$:$\mathbf{L_2}$ complexes. The values of $J(^{199}Hg^1H)$ were comparable to those observed for other Hg(II) complexes of thioether- and pyridine-containing ligands. Larger and longer range heteronuclear coupling constants with ^1H were observed for the 1:1 Hg(II) complex of $\mathbf{L_2}$ in comparison with the comparable Cd(II) complex. Also, slow exchange conditions could not be found for $Cd(ClO_4)_2$ complexes of $\mathbf{L_1^1}$. Weaker bonding, the typically smaller magnitude of $J(^{111/113}Cd^1H)$ or a combination of the two may have prevented access to slow exchange conditions. Heteronuclear couplings between ^{207}Pb and ^1H were never detected for the Pb(II) complex of $\mathbf{L_1^1}$, possibly due to weak bonding between Pb(II) and the thioether sulfur donor. Conditions for slow ligand exchange between Pb(II) complexes have not been studied systematically to determine favorable donor sets or solvents.

Further study of the zinc triad with multidentate ligands may provide insight into the toxicological potential of Hg(II) and Cd(II) and their implications as metallobioprobes. Heavy metals such as Hg(II), Cd(II) exhibit high affinity for sulfur donor ligands and more attention has been paid to metal-sulfur (thiolate) complexes as an inorganic model of metal-cysteine interaction. There are limited examples of Zn(II) binding to the thioether methionine in biological molecules. However, Hammes and Carrano reported the binding of Zn(II) to a thioether resulting from the methyl group transfer to a zinc thiolate.[94] Methionine coordination to iron and copper ions, on the other hand, is common in several classes of proteins, such as in the c and b type heme containing cytochromes, some iron dependent transcription regulators, and the blue copper and CuA cupredoxins. Although methionine residues are one of the less prevalent

amino acid side chains found bound to metals in the crystal structures of proteins, there are frequently methione residues just outside the coordination of metals that may become ligands for Hg(II) or Cd(II), further enhancing the stability of the substituted metal ion. ^{113}Cd and ^{119}Hg have been used to probe Cu-thioether coordination chemistry in various blue-copper proteins.[5,6,15] Larger and longer range $J(M^1H)$ in the $\mathbf{L_2}$ complex with Hg(II) compared to the Cd(II) complex indicates that ^{199}Hg NMR methods have some significant advantages as structural metallobioprobes over ^{113}Cd NMR methods. Moreover, thioether multidentate ligands may serve as selective heavy metal extraction agents and antagonists for treatment of heavy-metal positioning.[95] Additional coordination studies with thioether containing ligands are needed to evaluate the significance of methionine and other thioethers as targets for the toxic effects of heavy metal ions.

In spite of intense study, the detailed molecular mechanisms for the toxicology of heavy metals remain largely unresolved. While it is generally appreciated that Hg(II) has broader toxicological effects than Cd(II), the solution state research described here offers the fundamental insight that slow exchange of Hg(II) between multidentate coordination sites encountered relative to Cd(II) may contribute to the differences in their toxicological profile. Comparisons of the solutions state behavior of **1**, **2** and **3** suggest Hg(II) may be more effective competing for the native metal binding sites of specific proteins than Cd(II). Furthermore, slow ligand exchange for **1** suggests that Hg(II) may not require preformed metal binding sites with high coordination numbers to have toxic effects. The similarity of the solution-state coordination chemistry of $\mathbf{L_2}$ with Hg(II) and Cd(II) suggest that slow ligand exchange also depends on the specific donor sets. Additional

comparisons of the coordination behavior of the zinc triad with multidentate ligands possessing biologically relevant donor groups will help focus efforts to identify differences between the physiological targets of these metals.

REFFERENCES

1. Hutchison, A.R.; Atwood, D.A. *Journal of Chemical Crystallography* **2003**, *33*, 631.

2. Razmiafshari, M.; Kao, J.; d'Avignon, A.; Zawia, N.H. *Toxicology and Applied Pharmacology* **2001**, *172*, 1.

3. Sanchiz, J.; Esparza, P.; Villagra, D.; Dominguez, S.; Mederos, A.; Brito, F.; Araujo, L.; Sanchez, A.; Arrieta, J.M. *Inorganic Chemistry* **2002**, *41*, 6048.

4. Lane, T.W.; Morel, F.M.M. *Proceedings of the National Academy of Sciences* **2000**, *97*, 4627.

5. Utschig, L.M.; Wright, J.G.; Dieckmann, G.; Pecoraro, V.; O'Halloran, T.V. *Inorganic Chemistry* **1995**, *34*, 2497.

6. Summers, M.F. *Coordination Chemistry Reviews* **1988**, *86*, 43.

7. Bebout, D.C.; Garland, M.M.; Murphy, G.S.; Bowers, E.V.; Abelt, C.J.; Butcher, R.J. *Journal of the Chemical Society, Dalton Transactions* **2003**, 2578.

8. Bebout, D.C.; Bush, J.F., II; Shumann, E.M.; Viehweg, J.A.; Kastner, M.E.; Parrish, D.A.; Baldwin, S.M. *Journal of Chemical Crystallography* **2003**, *33*, 457.

9. Bebout, D.C.; Bush, J.F., II; Crahan, K.K.; Bowers, E.V.; Butcher, R.J. *Inorganic Chemistry* **2002**, *41*, 2529.

10. Bebout, D.C.; Stokes, S.W.; Butcher, R.J. *Inorganic Chemistry* **1999**, *38*, 1126.

11. Becker, A.; Schlichting, I.; Kabsch, W.; Groche, D.; Schultz, S.; Wagner, A.F.V. *Nature Structural Biology* **1998**, *5*, 1053.

12. Bebout, D.C.; DeLanoy, A.E.; Ehmann, D.E.; Kastner, M.E.; Parrish, D.A.; Butcher, R.J. *Inorganic Chemistry* **1998**, *37*, 2952.

13. Bebout, D.C.; Ehmann, D.E.; Trinidad, J.C.; Crahan, K.K.; Kastner, M.E.; Parrish, D. *Inorganic Chemistry* **1997**, *36*, 4257.

14. Berry, S.M.; Bebout, D.C.; Butcher, R.J. *Inorganic Chemistry* **2005**, *44*, 27.

15. Utschig, L.M.; Baynard, T.; Strong, C.; O'Halloran, T.V. *Inorganic Chemistry* **1997**, *36*, 2926.

16. Utschig, L.M.; Bryson, J.W.; O'Halloran, T.V. *Science* **1995**, *268*, 380.

17. Utschig, L.M.; Wright, J.G.; O'Halloran, T.V. *Methods in Enzymology* **1993**, *226*, 71.

18. Claudio, E.S.; Ter Horst, M.A.; Forde, C.E.; Stern, C.L.; Zart, M.K.; Godwin, H.A. *Inorganic Chemistry* **2000**, *39*, 1391.

19. Blake, P.R.; Lee, B.; Summers, M.F.; Park, J.B.; Zhou, Z.H.; Adams, M.W.W. *New Journal of Chemistry* **1994**, *18*, 387.

20. Gomis-Rueth, F.X.; Grams, F.; Yiallouros, I.; Nar, H.; Kuesthardt, U.; Zwilling, R.; Bode, W.; Stoecker, W. *Journal of Biological Chemistry* **1994**, *269*, 17111.

21. Church, W.B.; Guss, J.M.; Potter, J.J.; Freeman, H.C. *Journal of Biological Chemistry* **1986**, *261*, 234.

22. Anjali, K.S.; Vittal, J.J.; Dean, P.A.W. *Inorganica Chimica Acta* **2003**, *351*, 79.

23. Bell, N.A.; Branston, T.N.; Clegg, W.; Creighton, J.R.; Cucurull-Sanchez, L.; Elsegood, M.R.J.; Raper, E.S. *Inorganica Chimica Acta* **2000**, *303*, 220.

24. Castineiras, A.; Hiller, W.; Straehle, J.; Bravo, J.; Casas, J.S.; Gayoso, M.; Sordo, J. *Journal of the Chemical Society, Dalton Transactions* **1986**, 1945.

25. Spencer, D.J.E.; Blake, A.J.; Parsons, S.; Schroder, M. *Journal of the Chemical Society, Dalton Transactions* **1999**, 1041.

26. Brand, U.; Vahrenkamp, H. *Inorganic Chemistry* **1995**, *34*, 3285.

27. Ball, R.J.; Genge, A.R.J.; Radford, A.L.; Skelton, B.W.; Tolhurst, V.-A.; White, A.H. *Journal of the Chemical Society, Dalton Transactions* **2001**, 2807.

28. Marquez, V.E.; Anacona, J.R.; Hurtado, R.J.; De Delgado, G.D.; Roque, E.M. *Polyhedron* **1999**, *18*, 1903.

29. Canovese, L.; Visentin, F.; Chessa, G.; Uguagliati, P.; Santo, C.; Bandoli, G.; Maini, L. *Organometallics* **2003**, *22*, 3230.

30. Vinas, C.; Angles, P.; Sanchez, G.; Lucena, N.; Teixidor, F.; Escriche, L.; Casabo, J.; Piniella, J.F.; Alvarez-Larena, A.; Kivekaes, R.; Sillanpaeae, R. *Inorganic Chemistry* **1998**, *37*, 701.

31. Canovese, L.; Visentin, F.; Uguagliati, P.; Lucchini, V.; Bandoli, G. *Inorganica Chimica Acta* **1998**, *277*, 247.

32. Teixidor, F.; Sanchez-Castello, G.; Lucena, N.; Escriche, L.; Kivekas, R.; Sundberg, M.; Casabo, J. *Inorganic Chemistry* **1991**, *30*, 4931.

33. Teixidor, F.; Escriche, L.; Rodriguez, I.; Casabo, J.; Rius, J.; Molins, E.; Martinez, B.; Miravitlles, C. *Journal of the Chemical Society, Dalton Transactions* **1989**, 1381.

34. Escriche, L.; Sanz, M.; Casabo, J.; Teixidor, F.; Molins, E.; Miravitlles, C. *Journal of the Chemical Society, Dalton Transactions* **1989**, 1739.

35. Teixidor, F.; Escriche, L.; Casabo, J.; Molins, E.; Miravitlles, C. *Inorganic Chemistry* **1986**, *25*, 4060.

36. Stamp, S. *Honors Thesis*, The College of William & Mary **2004**.

37. Raymond, K.N. *Chemical & Engineering News* **1983**, *61*, 4.

38. Sheldrick, G.M. In; SHELXS 97 ed.; University of Göttingen, 1997.

39. Canovese, L.; Chessa, G.; Marangoni, G.; Pitteri, B.; Uguagliati, P.; Višentin, F. *Inorganica Chimica Acta* **1991**, *186*, 79.

40. Baker, W.; Buggle, K.M.; McOmie, J.F.W.; Watkins, D.A.M. *Journal of the Chemical Society, Abstracts* **1958**, 3594.

41. Tyeklar, Z.; Jacobson, R.R.; Wei, N.; Murthy, N.N.; Zubieta, J.; Karlin, K.D. *Journal of the American Chemical Society* **1993**, *115*, 2677.

42. Aakesson, R.; Sandstroem, M.; Staalhandske, C.; Persson, I. *Acta Chemica Scandinavica* **1991**, *45*, 165.

43. Marcus, S.T.; Bernhardt, P.V.; Grondahl, L.; Gahan, L.R. *Polyhedron* **1999**, *18*, 3451.

44. Blake, A.J.; Pasteur, E.C.; Reid, G.; Schroder, M. *Polyhedron* **1991**, *10*, 1545.

45. Nyburg, S.C.; Faerman, C.H. *Acta Crystallographica, Section B: Structural Science* **1985**, *B41*, 274.

46. Blake, A.J.; Reid, G.; Schroeder, M. *Polyhedron* **1990**, *9*, 2931.

47. Parra-Hake, M.; Larter, M.L.; Gantzel, P.; Aguirre, G.; Ortega, F.; Somanathan, R.; Walsh, P.J. *Inorganic chemistry* **2000**, *39*, 5400.

48. Neels, A.; Stoeckli-Evans, H. *Inorganic Chemistry* **1999**, *38*, 6164.

49. Glerup, J.; Goodson, P.A.; Hodgson, D.J.; Michelsen, K.; Nielsen, K.M.; Weihe, H. *Inorganic Chemistry* **1992**, *31*, 4611.

50. Matsuda, K.; Takayama, K.; Irie, M. *Inorganic Chemistry* **2004**, *43*, 482.

51. Stec, B.; Hehir, M.J.; Brennan, C.; Nolte, M.; Kantrowitz, E.R. *Journal of Molecular Biology* **1998**, *277*, 647.

52. Korkhin, Y.; Kalb, A.J.; Peretz, M.; Bogin, O.; Burstein, Y.; Frolow, F. *Journal of Molecular Biology* **1998**, *278*, 967.

53. Fabiane, S.M.; Sohi, M.K.; Wan, T.; Payne, D.J.; Bateson, J.H.; Mitchell, T.; Sutton, B.J. *Biochemistry* **1998**, *37*, 12404.

54. Hyvonen, M.; Saraste, M. *EMBO Journal* **1997**, *16*, 3396.

55. Helm, M.L.; Combs, C.M.; VanDerveer, D.G.; Grant, G.J. *Inorganica Chimica Acta* **2002**, *338*, 182.

56. Blake, A.J.; Danks, J.P.; Fallis, I.A.; Harrison, A.; Li, W.-S.; Parsons, S.; Ross, S.A.; Whittaker, G.; Schroder, M. *Journal of the Chemical Society, Dalton Transactions* **1998**, 3969.

57. Atkinson, N.; Blake, A.J.; Drew, M.G.B.; Forsyth, G.; Gould, R.O.; Lavery, A.J.; Reid, G.; Schroeder, M. *Journal of the Chemical Society, Dalton Transactions* **1992**, 2993.

58. Atkinson, N.; Blake, A.J.; Drew, M.G.B.; Forsyth, G.; Lavery, A.J.; Reid, G.; Schroder, M. *Journal of the Chemical Society, Chemical Communications* **1989**, 984.

59. De Vries, N.; Reedijk, J. *Inorganic Chemistry* **1991**, *30*, 3700.

60. McAuley, A.; Subramanian, S. *Inorganic Chemistry* **1990**, *29*, 2830.

61. Chandrasekhar, S.; McAuley, A. *Inorganic Chemistry* **1992**, *31*, 2234.

62. Blake, A.J.; Reid, G.; Schroeder, M. *Journal of the Chemical Society, Dalton Transactions* **1994**, 3291.

63. Chiou, S.-J.; Ge, P.; Riordan, C.G.; Liable-Sands, L.M.; Rheingold, A.L. *Chemical Communications* **1999**, 159.

64. Adhikary, B.; Liu, S.; Lucas, C.R. *Inorganic Chemistry* **1993**, *32*, 5957.

65. Adhikary, B.; Liu, S.; Lucas, C.R. *Inorganica Chimica Acta* **1997**, *261*, 15.

66. Grillo, V.A.; Gahan, L.R.; Hanson, G.R.; Stranger, R.; Hambley, T.W.; Murray, K.S.; Moubaraki, B.; Cashion, J.D. *Journal of the Chemical Society, Dalton Transactions* **1998**, 2341.

67. Atkinson, N.; Lavery, A.J.; Blake, A.J.; Reid, G.; Schroeder, M. *Polyhedron* **1990**, *9*, 2641.

68. Addison, A.W.; Rao, T.N.; Reedijk, J.; Van Rijn, J.; Verschoor, G.C. *Journal of the Chemical Society, Dalton Transactions* **1984**, 1349.

69. Moghimi, A.; Shokrollahi, A.; Shamsipur, M.; Aghabozorg, H.; Ranjbar, M. *Journal of Molecular Structure* **2004**, *701*, 49.

70. Bebout, D.C.; Bush, J.F., II; Crahan, K.K.; Kastner, M.E.; Parrish, D.A. *Inorganic Chemistry* **1998**, *37*, 4641.

71. Bermejo, E.; Castineiras, A.; Garcia, I.; West, D.X. *Polyhedron* **2003**, *22*, 1147.

72. Wang, Q.-H.; Long, D.-L.; Huang, J.-S. *Polyhedron* **1998**, *17*, 3665.

73. Matthews, C.J.; Clegg, W.; Heath, S.L.; Martin, N.C.; Hill, M.N.S.; Lockhart, J.C. *Inorganic Chemistry* **1998**, *37*, 199.

74. Pazderski, L.; Szlyk, E.; Wojtczak, A.; Kozerski, L.; Sitkowski, J.; Kamienski, B. *Journal of Molecular Structure* **2004**, *697*, 143.

75. Loi, M.; Graf, E.; Hosseini, M.W.; De Cian, A.; Fischer, J. *Chemical Communications* **1999**, 603.

76. Yang, F.-A.; Chen, J.-H.; Hsieh, H.-Y.; Elango, S.; Hwang, L.-P. *Inorganic Chemistry* **2003**, *42*, 4603.

77. Das, S.; Hung, C.-H.; Goswami, S. *Inorganic Chemistry* **2003**, *42*, 5153.

78. Karlin, S.; Zhu, Z.-Y.; Karlin, K.D. *Biochemistry* **1998**, *37*, 17726.

79. Garcia-Saez, I.; Hopkins, J.; Papamicael, C.; Franceschini, N.; Amicosante, G.; Rossolini Gian, M.; Galleni, M.; Frere, J.-M.; Dideberg, O. *Journal of biological chemistry* **2003**, *278*, 23868.

80. Chantalat, L.; Leroy, D.; Filhol, O.; Nueda, A.; Benitez, M.J.; Chambaz, E.M.; Cochet, C.; Dideberg, O. *EMBO Journal* **1999**, *18*, 2930.

81. Arca, M.; Blake, A.J.; Lippolis, V.; Montesu, D.R.; McMaster, J.; Tei, L.; Schroder, M. *European Journal of Inorganic Chemistry* **2003**, 1232.

82. Ferlay, S.; Jouaiti, A.; Loi, M.; Hosseini, M.W.; De Cian, A.; Turek, P. *New Journal of Chemistry* **2003**, *27*, 1801.

83. Agnus, Y.; Louis, R.; Weiss, R. *Journal of the American Chemical Society* **1979**, *101*, 3381.

84. Weber, G. *Inorganica Chimica Acta* **1982**, *58*, 27.

85. Nekola, H.; Rehder, D. *Inorganica Chimica Acta* **2002**, *337*, 467.

86. Schlager, O.; Wieghardt, K.; Grondey, H.; Rufinska, A.; Nuber, B. *Inorganic Chemistry* **1995**, *34*, 6440.

87. Allred, R.A.; Arif, A.M.; Berreau, L.M. *Journal of the Chemical Society, Dalton Transactions* **2002**, 300.

88. Jubert, C.; Mohamadou, A.; Marrot, J.; Barbier, J.-P. *Journal of the Chemical Society, Dalton Transactions* **2001**, 1230.

89. Bruce, J.I.; Donlevy, T.M.; Gahan, L.R.; Kennard, C.H.; Byriel, K.A. *Polyhedron* **1996**, *15*, 49.

90. Makowska-Grzyska Magdalena, M.; Jeppson Peter, C.; Allred Russell, A.; Arif Atta, M.; Berreau Lisa, M. *Inorganic chemistry* **2002**, *41*, 4872.

91. Basu Baul, T.S.; Lycka, A.; Butcher, R.; Smith, F.E. *Polyhedron* **2004**, *23*, 2323.

92. McCrindle, R.; Ferguson, G.; McAlees, A.J.; Parvez, M.; Ruhl, B.L.; Stephenson, D.K.; Wieckowski, T. *Journal of the Chemical Society, Dalton Transactions* **1986**, 2351.

93. McWhinnie, W.R.; Monsef-Mirzai, Z.; Perry, M.C.; Shaikh, N.; Hamor, T.A. *Polyhedron* **1993**, *12*, 1193.

94. Hammes, B.S.; Carrano, C.J. *Chemical Communications* **2000**, 1635.

95. Setzer, W.N.; Tang, Y.; Grant, G.J.; VanDerveer, D.G. *Inorganic Chemistry* **1992**, *31*, 1116.

VITA

Wei Lai

Wei Lai was born in Fushun, Liaoning of China on June 13, 1976. She graduated from Liaoning Normal University, China in July 1999 with a B.S. degree in Chemistry. In July 2002, She received her M.S. degree in Physical Chemistry from Liaoning Normal University.

She entered the College of William and Mary as a graduate assistant in Department of Chemistry in May of 2004 and completed all the requirements for a M.S. degree in July of 2005.